Atmospheric
Chemistry
and Physics
Discussions

Open Access

Transport of anthropogenic and biomass burning aerosols from Europe to the Arctic during spring 2008

L. Marelle[1,2], J.-C. Raut[1], J. L. Thomas[1], K. S. Law[1], B. Quennehen[1], G. Ancellet[1], J. Pelon[1], A. Schwarzenboeck[3], and J. D. Fast[4]

[1]Sorbonne Universités, UPMC Univ. Paris 06; Université Versailles St-Quentin; CNRS/INSU, LATMOS-IPSL, Paris, France
[2]TOTAL S.A/DS, Tour Coupole, 92078 Paris La Defense, France
[3]Laboratoire de Météorologie Physique, UMR6016, Université Blaise Pascal, CNRS, Aubière, France
[4]Pacific Northwest National Laboratory, Richland, Washington, USA

Correspondence to: L. Marelle (louis.marelle@latmos.ipsl.fr)

Abstract

During the POLARCAT-France airborne campaign in April 2008, pollution originating from anthropogenic and biomass burning emissions was measured in the European Arctic. We compare these aircraft measurements with simulations using the WRF-Chem model to investigate model representation of aerosols transported from Europe to the Arctic. Modeled $PM_{2.5}$ is evaluated using EMEP measurements in source regions and POLARCAT aircraft measurements in the Scandinavian Arctic, showing a good agreement, although the model overestimates nitrate and underestimates organic carbon in source regions. Using WRF-Chem in combination with the Lagrangian model FLEXPART-WRF, we find that during the campaign the research aircraft sampled two different types of European plumes: mixed anthropogenic and fire plumes from eastern Europe and Russia transported below 2 km, and anthropogenic plumes from central Europe uplifted by warm conveyor belt circulations to 5–6 km. Both modeled plume types had significant wet scavenging (> 50 % PM_{10}) during transport. Modeled aerosol vertical distributions and optical properties below the aircraft are evaluated in the Arctic using airborne LIDAR measurements. Evaluating the regional impacts in the Arctic of this event in terms of aerosol vertical structure, we find that during the 4 day presence of these aerosols in the lower European Arctic (< 75° N), biomass burning emissions have the strongest influence on concentrations between 2.5 and 3 km altitudes, while European anthropogenic emissions influence aerosols at both lower (∼ 1.5 km) and higher altitudes (∼ 4.5 km). As a proportion of $PM_{2.5}$, modeled black carbon and $SO_4^=$ concentrations are more enhanced near the surface. The European plumes sampled during POLARCAT-France were transported over the region of springtime snow cover in Northern Scandinavia, where they had a significant local atmospheric warming effect. We find that, during this transport event, the average modeled top of atmosphere (TOA) shortwave direct and semi-direct radiative effect (DSRE) north of 60° N over snow and ice-covered surfaces reaches +0.58 W m^{-2}, peaking at +3.3 W m^{-2} at noon over Scandinavia and Finland.

1 Introduction

Arctic haze, which is present during winter and spring, is a well known phenomenon that includes elevated concentrations of anthropogenic aerosols transported to the Arctic region (e.g. Rahn et al., 1977; Quinn et al., 2007). It was identified for the first time in the 1950s, when pilots experienced reduced visibility in the springtime North American Arctic (Greenaway, 1950; Mitchell, 1957). Further analysis showed that Arctic haze aerosols are mostly composed of sulfate, as well as organic matter, nitrate, sea salt, and black carbon (e.g. Quinn et al., 2002). Since local Arctic emissions are rather low, most air pollutants in the Arctic originate from transport from the mid-latitudes (Barrie, 1986). In late winter and early spring, Eurasian emissions can be efficiently transported at low-level in the Arctic (Rahn, 1981), while removal processes are particularly slow (Shaw, 1995; Garrett et al., 2011), causing elevated pollution concentrations in the lower troposphere. Surface aerosol concentrations in the Arctic are mostly influenced by European and West Asian emissions, while East Asian emissions have a larger influence in the upper troposphere (Fisher et al., 2011). Eurasian biomass burning emissions are thought to be major sources of Arctic pollution (Stohl, 2006; Warneke et al., 2010), but the magnitude of this contribution is still uncertain.

Aerosols play a key role in the climate system, through absorption and scattering of solar radiation (e.g. Haywood et Shine, 1995; Charlson et al., 1992), and their impacts on cloud formation (Ackerman et al., 2000; Twomey, 1977). In the Arctic, several processes enhance the radiative impact of aerosols, including soot deposition on snow (Flanner et al., 2007), increased long wave emissivity in clouds in polluted conditions (Garret and Zhao, 2006), and the increased atmospheric heating effect of low absorbing aerosols over snow or ice covered surfaces (Pueschel and Kinne, 1995; Haywood and Shine, 1995). Modeling studies by Shindell and Faluvegi (2009) and Jacobson, (2010) suggest that a good representation of aerosol composition and optical properties is critical to understand the Arctic energy budget. However, it is well known that aerosols amounts and properties in the Arctic are not well represented in global

Title Page

Abstract | Introduction

Conclusions | References

Tables | Figures

|◄ | ►|

◄ | ►

Back | Close

Full Screen / Esc

Printer-friendly Version

Interactive Discussion

chemical-transport models. For example, Schwarz et al. (2010) showed that black carbon in global simulations does not agree well with observations in the Arctic and varies greatly between models. This discrepancy, especially at high altitudes, may be caused, in part, by insufficient rainout (e.g. Wang et al., 2013).

To improve our understanding about air pollution in the Arctic, several airborne campaigns were conducted in the Arctic region during the International Polar Year in 2008 in the framework of POLARCAT (POLar study using Aircraft, Remote sensing, surface measurements and models, of Climate, chemistry, Aerosols, and Transport, see Law et al., 2014). As part of the international project POLARCAT, the POLARCAT-France spring campaign took place from 30 March to 14 April 2008, based in Kiruna, Sweden (67.8° N, 20.2° E). This campaign focused on Arctic cloud-aerosol interactions, satellite measurement validation, and transport of pollution plumes from mid-latitudes to the Arctic. During the campaign, several anthropogenic and biomass burning plumes originating in Europe and Asia were transported to the flight area and sampled during flights in April 2008 (Adam de Villiers et al., 2010; Quennehen et al., 2012). Adam de Villiers et al. (2010) analyzed the optical properties of aerosol plumes measured by airborne and spaceborne LIDAR, and Quennehen et al. (2012) studied aerosol ageing from size distributions measured in situ during POLARCAT-France spring. These studies pointed the need for modeling to quantify the influence of different processes and sources on aerosols observed during the campaign.

The present study aims to improve our understanding about aerosol originating from Europe. In particular, we investigate the role of anthropogenic and biomass burning sources, transport pathways, aerosol ageing, and processes controlling the vertical distribution of aerosol plumes transported to the European Arctic in spring, and how they impact the aerosol burden and the aerosol radiative effect in this region. To achieve this objective, measurements from the POLARCAT-France airborne campaign in the Scandinavian Arctic in April 2008 are analyzed in combination with simulations using the regional WRF-Chem model to investigate cases of aerosol transport from Europe to the Arctic. In Sect. 2, we describe the methods used in our study, including a descrip-

tion of the POLARCAT-France spring airborne aerosols measurements, and the EMEP ground based aerosol measurements used to validate the model over European source regions. Section 2 also includes an overview of the modeling tools employed, WRF-Chem and FLEXPART-WRF, and describes the simulations performed in this study.

5 In Sect. 3, we present the synoptic scale meteorological situation over Europe during the campaign, and how this situation impacted long-range aerosol transport from Europe to the Arctic. In Sect. 4, the performance of the WRF-Chem simulation is evaluated using POLARCAT-France spring meteorological measurements and ground based aerosol measurements in source regions. In Sect. 5, modeled aerosol physical and op-

10 tical properties are compared to POLARCAT-France spring airborne in situ and LIDAR measurements. We also investigate in Sect. 5 the sources of aerosols observed during the campaign. The results are used in Sect. 6 to evaluate the regional impact of this transport event in terms of aerosols burden and direct radiative effects.

2 Methods

15 ### 2.1 POLARCAT-France spring campaign airborne measurements

During POLARCAT-France, the French ATR-42 research aircraft payload included two instruments to measure the particle size distribution: a Scanning Mobility Particle Sizer (SMPS, size range 20 to 467 nm, 88 channels) and a GRIMM Optical Particle Counter (OPC, size range 0.1 to 2 µm, 8 channels). For the full size distributions (20 nm to 2 µm),

20 data from the two instruments are combined as described in Quennehen et al. (2012). The ATR-42 was equipped with a Counterflow Virtual Impactor (CVI) inlet (Schwarzenboeck et al., 2000) to sample aerosol particles and cloud droplets. In clouds, the CVI inlet was activated to remove interstitial aerosols and study cloud droplets only. Therefore, aerosol size distributions are only available out of clouds. However, clouds mostly

25 impacted in-situ measurements at lower altitudes (< 2 km) and data is available for most periods of interest for modeling long-range transport of aerosols to the region

(88 % data coverage above 1.5 km). $PM_{2.5}$ concentrations along the flight track are estimated by integrating the size distributions (20 nm to 2 µm), assuming that all particles are spherical and have a density of 1700 kg m^{-3} (Quennehen et al., 2011). The contribution of particles in the 2–2.5 µm diameter range to $PM_{2.5}$ is missing from this estimation. However, we determine it is negligible, because 94 % of the measured 20 nm to 2 µm mass distribution is located in the lower size range 20 nm to 1.6 µm, and because large particles are unlikely to be transported over long distances.

During the campaign, airborne aerosol LIDAR profiles were measured below or above the aircraft by the LNG instrument (LIDAR LEANDRE Nouvelle Génération) (Flamant and Pelon, 1996; Adam de Villiers et al., 2010; Ancellet, 2014). Specifically, the LNG instrument measured aerosol optical properties at two wavelengths (532 and 1064 nm) providing information about the location of aerosol layers vertically (in our case below the aircraft). The vertical resolution of the data presented is 30 m (4 point average) and the horizontal resolution is 450 m (average of 100 LIDAR shots). In this work, we use the LNG measurements to study the spatial structure of aerosol layers below the aircraft and to analyze the representation of these aerosol layers in regional chemical transport modeling. For this purpose, we use the LNG measurements to calculate the pseudo backscatter ratio (PBR), defined as the ratio of the measured LIDAR total attenuated backscatter (including Rayleigh and aerosol contributions) to simulated molecular backscatter at a certain wavelength. The uncertainty for this ratio is estimated to be 10 % for the 532 nm channel and 20 % for the 1064 nm channel by Adam de Villiers et al. (2010). For this reason, we only use the 532 nm PBR in this study. In moderately polluted conditions (as observed during POLARCAT-France spring campaign), the PBR is close to the true backscatter ratio, defined as $R_T = \frac{(\beta_A + \beta_M)}{\beta_M}$, where β_A is the aerosol backscatter coefficient and β_M is the molecular backscatter coefficient, noting that the true backscatter ratio is equal to 1 in clear sky conditions, and is greater than 1 in aerosol layers. Several aerosol plumes were sampled in situ and measured by LIDAR during three flights on 9, 10 and 11 April 2008. The associated flight tracks,

over northern Norway and the Norwegian Sea/Barents Sea region, are represented in Fig. 1.

2.2 EMEP ground based measurements

The European Monitoring and Evaluation Programme (EMEP) network of ground-based measurements includes both aerosol $PM_{2.5}$ mass and aerosol chemical composition (available online from the EMEP database – http://www.nilu.no/projects/ccc/). Stations from the EMEP network are typically outside of urban centers and are intended to represent background and/or aged aerosol properties, as they are not co-located with large emissions sources. We use the EMEP measurements to evaluate model aerosols from 1 April to 11 April 2008, using data from stations with either daily or hourly data. In addition, stations are excluded if they have less than 75 % data coverage during this period, and OC or BC measurements are excluded because of the lack of spatial coverage of measurements (4 stations for BC, 5 for OC). The locations of stations used for model comparison are shown in Fig. 1, including stations that measure $PM_{2.5}$ (33 stations) and stations that measure aerosol mass of $SO_4^=$, NH_4^+, and NO_3^- (34, 31, and 28 stations respectively). The average data coverage for selected stations is 98 %.

2.3 Model calculations: WRF-Chem and FLEXPART-WRF

2.3.1 WRF-Chem

Regional chemical transport model simulations are performed with the version 3.5.1 of the WRF-Chem (Weather Research and Forecasting, including Chemistry) model to provide further insight into the POLARCAT-France spring aerosol measurements. WRF-Chem is a fully coupled, online meteorological and chemical-transport mesoscale model (Grell et al., 2005; Fast et al., 2006). It has been successfully used in previous studies focused on the Arctic region (Sessions et al., 2011; Thomas et al., 2013) and

to analyze airborne aerosols measurements (e.g. Fast et al., 2012). The model setup including the representation of the planetary boundary layer, surface, radiative properties, convection, microphysics, gas phase chemistry, and aerosols is shown in Table 1. Specifically, gas-phase reactions were simulated with the CBM-Z mechanism (Carbon Bond Mechanism, version Z) (Zaveri and Peters, 1999) and aerosols are represented using the 8 bin sectional aerosol model MOSAIC (Model for Simulating Aerosol Interactions and Chemistry, Zaveri et al., 2008). MOSAIC aerosol processes include nucleation, evaporation, coagulation, condensation, cloud chemistry, aerosol/cloud interactions, dry deposition, and within and below cloud wet scavenging. Eight bins represent the size distribution of each aerosol species between 39 nm and 10 µm. Interstitial and cloud-borne aerosol particles are treated explicitly, and modeled aerosols can be activated or resuspended depending on saturation, particle sizes and aerosol composition. Aqueous chemistry in clouds is based on Fahey and Pandis (2001), and includes oxidation of S(IV) by H_2O_2, O_3, and other radicals, as well as non-reactive uptake of NH_3, HNO_3, HCl, and other trace gases. Nucleation is based on Wexler et al. (1994). The CBM-Z-MOSAIC 8 bin scheme is not coupled to a secondary organic aerosol (SOA) scheme in our version of WRF-Chem (3.5.1). Furthermore, current SOA mechanisms are still highly uncertain (e.g. Hodzic et al., 2010; Gustafson et al., 2011), and SOA formation is likely to be low in Europe and at high latitudes in early April. Because of this, our simulation did not include SOA formation. MOSAIC considers aerosols as internally mixed in each bin, and in our simulations optical properties are calculated using volume averaging.

The simulation domain, focused on the POLARCAT-France spring flights, is shown in Fig. 1 and covers Europe north of 40° N and west of 70° E. The spatial resolution is 30 km×30 km horizontally, with 50 vertical levels up to 50 hPa. Anthropogenic emissions were taken from the HTAPv2 0.1° × 0.1° inventory (http://edgar.jrc.ec.europa.eu/htap_v2/index.php?SECURE=123). HTAP VOCs are given as a bulk VOC mass, and are distributed into CBM-Z emission categories assuming the speciation of UK VOCs determined by Murrels et al. (2010). Time profiles are applied to anthropogenic emissions

Title Page

Abstract | Introduction

Conclusions | References

Tables | Figures

|◄ | ►|

◄ | ►

Back | Close

Full Screen / Esc

Printer-friendly Version

Interactive Discussion

to account for the daily and weekly cycle of each emission sector (Denier van der Gon et al., 2011). Fire emissions are from the FINN v1 inventory (Wiedinmyer et al., 2006, 2011), and are injected in altitude by an online plume rise model described in Freitas et al. (2007). Figure 2 shows black carbon (BC), organic carbon (OC), and sulfur oxides (SO$_x$) emissions during our simulation, from both anthropogenic sources (panels A, B and C) and biomass burning sources (panels D, E and F). In-domain biomass burning emission totals are 13 kilotons (kt) for SO$_x$, 12 kt for BC and 75 kt for OC. For anthropogenic emissions, emission totals are 575 kt for SO$_x$, 21 kt for BC and 46 kt for OC. Anthropogenic emissions are stronger in Western and Central Europe, especially in Poland and Slovakia. Biomass burning emissions are located in the eastern part of the domain, because of intense agricultural fires in Ukraine, Russia and Kazakhstan during early April 2008 (Warneke et al., 2009). Biogenic emissions are calculated online in WRF-Chem by the model MEGAN (Guenther et al., 2006). Finally, sea salt aerosol emissions are calculated online, while mineral dust emissions are not included.

Boundary and initial meteorological conditions in the simulation are given by the global NCEP Final Analysis (FNL), and WRF-Chem temperature, humidity and winds are nudged every 6 hours to the reanalysis above the atmospheric boundary layer. Trace gases and aerosol initial and boundary conditions (updated every 6 h) are taken from the global chemical transport model MOZART 4 (Emmons et al., 2010).

WRF-Chem simulations include a control run (CTL) from 00:00 UTC 1 April to 00:00 UTC 12 April using the model and emissions as described above. We also perform 4 sensitivity simulations for the same period to investigate the sources, processes along transport and regional impacts of aerosols sampled during POLARCAT: (1) removing the HTAPv2 emissions (NOANTHRO), (2) without biomass burning emissions (NOFIRES), (3) a simulation with wet scavenging turned off (NOWETSCAV), and (4) a simulation with the aerosol direct interaction with short wave radiation turned off (NODIRECT). The NOANTHRO and NOFIRE simulations are used to estimate the contribution of European anthropogenic and biomass burning emissions to Arctic aerosols measured during POLARCAT. The NOWETSCAV simulation allows us to quantify the

Title Page

Abstract | Introduction

Conclusions | References

Tables | Figures

|◄ | ►|

◄ | ►

Back | Close

Full Screen / Esc

Printer-friendly Version

Interactive Discussion

magnitude of the wet scavenging of aerosols during their transport from Europe to the Arctic. The NODIRECT simulation is used to estimate the direct and semi-direct shortwave radiative effect (DSRE) of aerosols associated with this transport event.

To compare simulations with airborne LIDAR measurements, modeled backscatter ratio profiles at the plane position are calculated by using the aerosol backscattering coefficient at 400 nm simulated by WRF-Chem. This coefficient is computed from the method of Toon and Ackerman (1981), using a bulk, volume averaged, refractive index derived from the modeled size distribution (Bond et al., 2006). The backscattering coefficient is then estimated at 532 nm by using the simulated Angström exponent, and the effect of aerosol transmission is ignored because aerosol optical depths of observed layers were low (< 4 %) during POLARCAT-France (Adam de Villiers et al., 2010). The backscatter ratio is calculated following the definition in Sect. 2.1, where the molecular backscattering is estimated by an empirical formulation of the Rayleigh scattering (Nicolet, 1984) using meteorological profiles from the CTL simulation.

2.3.2 FLEXPART-WRF

We also use FLEXPART-WRF, a Lagrangian particle dispersion model (Brioude et al., 2013) adapted from the model FLEXPART (Stohl et al., 2005), to study air mass origins and transport processes using WRF meteorological forecasts. In this study, we use FLEXPART-WRF in backward mode to study the origin and transport pathways of plumes measured during the POLARCAT-France spring campaign, and to provide insight into the WRF-Chem representation of aerosols. The meteorological fields from the WRF-Chem simulation CTL described in 3.1 are used as input. Every minute, 10 000 particles are released along the aircraft flight tracks in a volume 10 km × 10 km (horizontally) and 400 m (vertically). Each of the simulations is run backwards for 7 days to track the air mass origin over the source regions of interest (transport times are typically less than 7 day). Specifically, we use FLEXPART-WRF Potential Emission Sensitivity (PES) to study source–receptor relationships for air measured by the ATR-42 as part of the POLARCAT-France spring flights.

3   Meteorological context during the spring POLARCAT-France campaign

Long-range transport of aerosol from Europe to the Arctic is usually associated with specific synoptic meteorological situations over Europe, causing large scale meridional transport (e.g. Iversen and Joranger, 1985). In order to investigate the origin and transport of aerosols measured during the POLARCAT-France spring campaign, the synoptic meteorological situation during the campaign as represented by WRF-Chem is shown in Fig. 3. Specifically, WRF-Chem simulated geopotential height contours and wind arrows (700 hPa) are shown from 6 to 11 April 2008. A similar figure showing wind speed at 700 hPa instead of geopotential height is shown in the Supplement, Fig. S1. A low pressure over the North Sea and a high pressure over southwestern Russia and Kazakhstan caused southerly winds over Central and Eastern Europe from 6–8 April. On 8 April, the North Sea low pressure moved over the Baltic Sea, pushing those southerly winds deeper into the Scandinavian Arctic. On 9 April, the low pressure weakened and moved over Finland, while a deep trough formed over the Kara Sea, stopping northward transport and producing strong westerly winds over Europe and western Russia through the end of the aircraft campaign on 11 April.

Aerosols and other pollution are transported from lower latitudes in Europe in these synoptic meteorological systems, which determine the main pollution transport pathways. We show vertically integrated black carbon as a proxy for pollution transported during this time period in Fig. 4 (CTL simulation). The intersection of the low over the North Sea and the high located over Russia lead to the northward transport of a large polluted air mass from Central and Eastern Europe. A portion of this air mass was carried eastward at mid-latitudes, while another portion reached Arctic Scandinavia on 8 to 9 April. This polluted air mass was sampled by POLARCAT-France flights on 9, 10 and 11 April 2008, the flights that are the main focus of this study. However, this air mass did not penetrate deep into the Arctic and mix significantly with Arctic air due to the position of the polar front (Ancellet et al., 2014). On 10–11 April, the Arctic outflow intensified in the Barents and Norwegian Sea, slowly transporting the polluted European

air back to lower latitudes. On 10–11 April, pollution (represented as elevated BC) can be seen entering the simulation domain from the northern boundary over Svalbard (in our simulations via the MOZART boundary conditions), and crossing the POLARCAT flight track on 11 April. This last polluted air mass is not the focus of the present study and has been identified by as a mixed anthropogenic and biomass burning plume orig-inating from northeast Asia. It has already been studied in detail by Adam de Villiers et al. (2010) and Quennehen et al. (2012).

4   Model validation

Results from WRF-Chem are compared to POLARCAT-France measurements of tem-perature, relative humidity, wind speed, and wind direction (CTL simulation) for the POLARCAT-France flights included in our study. This comparison is presented in Fig. 5. Modeled and measured quantities are in good agreement with the exception of fine scale features that are not reproduced by the model due to the horizontal grid spac-ing (30 km). In particular, we note that relative humidity (RH) is well reproduced by the model ($R^2 > 0.88$). Pilinis et al. (1995) showed that RH, through aerosol water uptake, is a key parameter for modeling aerosol optical properties. The main discrepancies are between the measured and modeled wind speeds on 10 April 2008, in which high winds were observed below 1 km (middle portion of the flight) over the Norwegian Sea. However, discrepancies between modeled and measured wind speeds in the marine boundary layer over the Norwegian Sea during this portion of the fight do not impact the results for the pollution events we focus on, which were encountered higher up in the Scandinavian free troposphere and were emitted over continental Europe. The model performance in the Arctic troposphere indicates that the model captures the changing meteorological conditions in the European Arctic at the end of the POLARCAT-France spring campaign (discussed earlier in Sect. 3). This provides confidence that plume transport and dispersion are adequately represented to study aerosol transport and processing.

We evaluate model performance over the European source regions by comparing background aerosol levels from the EMEP network with model results (CTL simulation) extracted at the station locations. Figure 6 shows the comparison for $PM_{2.5}$, $SO_4^=$, NO_3^-, and NH_4^+, daily averaged for all stations. Error bars show the standard deviation between stations for both measured and modeled aerosols. Overprediction of aerosols on 1 April for $PM_{2.5}$, NO_3^-, and NH_4^+ correspond to positive biases for these species in the initial conditions (MOZART4), but WRF-Chem results are in better agreement with measurements after one day of simulation. This first day is considered as model spin-up, and is excluded from further analysis. We evaluate the model performance in reproducing European background aerosol levels in terms of Normalized Mean Bias (NMB). It is defined as $NMB = 100\% \times 1/N \times \sum_{i=1}^{N} (M_i - O_i)/O_i$, where M_i and O_i are modeled and observed daily values, averaged over all sites, and the summation is over the $N = 10$ days between 2 and 11 April. $PM_{2.5}$ levels are well reproduced by the model (NMB = −0.9 %). There are more significant differences in measured and modeled aerosol composition: while $SO_4^=$ agrees well with measurements (NMB = −0.6 %), NO_3^- (NMB = +107 %) and NH_4^+ (NMB = +53 %) are overestimated. This suggests that the overestimation of NO_3^- and NH_4^+ might be compensated by an underestimation of organic carbon (OC) aerosols. Due to a lack of available OC measurement from EMEP stations for this period, this hypothesis cannot be verified. If we use the very limited EMEP OC data (5 stations, 67 % coverage), we find that OC is indeed underestimated for those stations (NMB = −38 %). This underestimation could be caused, in part, by the fact that SOA is not included in our model run. However, we note that previous studies including SOA can report errors on OC of the same magnitude or larger (e.g. −74 % in Tuccella et al., 2012).

The overestimation of NO_3^- and NH_4^+ and underestimation of OC by WRF-Chem in Europe were also seen in the simulations of Tuccella et al. (2012), using different emissions as well as gas and aerosol schemes. That study suggested the discrepancy was due to missing aqueous reactions causing an underestimation of sulfate

Transport of European aerosols to the Arctic in spring

L. Marelle et al.

Title Page

Abstract	Introduction
Conclusions	References
Tables	Figures

|◄ | ►|

◄ | ►

Back | Close

Full Screen / Esc

Printer-friendly Version

Interactive Discussion

formation, leading to less neutralization of ammonium by sulfate and favoring the formation of ammonium nitrate (see Meng et al., 1997). It also highlighted the possible role of uncertainties in the simplified wet scavenging scheme used for that study. Our study includes a more complete wet scavenging scheme and the full range of aqueous reactions included in MOSAIC, keeping in mind that cloud/aerosol interaction processes in MOSAIC are only accounted for in dynamically resolved clouds, which should be underestimated in our simulation (30 km horizontal resolution). The inclusion of these processes, and the use of different anthropogenic emissions (EMEP in Tuccella et al. (2012) vs. HTAPv2 in the present study) can explain the better agreement on sulfate compared to Tuccella et al. (2012). However, this better agreement also means that, in our case, sulfate concentrations do not drive the overestimation of modeled ammonium and nitrate. Using EMEP measurements of ammonia (19 stations) and NO_x (10 stations), we found that NH_3 is overestimated by a factor of 2 in our simulation (NMB = +108 %) while NO_x is slightly underestimated (NMB = −23 %). This overestimation of NH_3 could cause of an enhanced formation of ammonium nitrate, which would explain the model overestimation of ammonium and nitrate.

While the CTL simulation is able to reproduce $PM_{2.5}$ levels observed in source regions, this good performance is due in part to compensating effects between different chemical components of the aerosols. The hygroscopy of OC (0.14) is lower than the one for NO_3^- and NH_4^+ (0.5) in MOSAIC. This means that the underestimation of OC in our simulation might lead to overestimated aerosol activation in clouds and wet scavenging. However, refractive indices for OC, NH_4NO_3 and $2NH_4SO_4$ are close (1.45, 1.50, 1.47 in MOSAIC), meaning that compensation between these different components should not have a strong impact on modeled aerosol optical properties, and that our model represents European aerosols sufficiently well to investigate their radiative effects in the Arctic.

Full Screen / Esc

Printer-friendly Version

Interactive Discussion

5 The origin and properties of springtime aerosols during POLARCAT-France

In this section, modeled aerosols in the Arctic are compared with POLARCAT-spring measurements, to investigate in detail the aerosol transport event from Europe to the Arctic. We combine WRF-Chem simulations with FLEXPART-WRF to identify the source regions and transport pathways of plumes sampled during the campaign, and show how they impact processes along transport and the vertical structure of Arctic pollution. First, aerosol particles detected in plumes in April 2008 are described in terms of mass concentrations, chemical composition and number size distributions. The role of transport pathways and wet scavenging along transport on those properties is also investigated. Aerosol optical properties are then used to quantify the vertical distribution of aerosols as a function of their emission sources.

5.1 Modeling aerosols measured in situ on 9, 10 and 11 April 2008

POLARCAT-France measured (in-situ) $PM_{2.5}$ is compared with modeled $PM_{2.5}$ interpolated in space (model results using hourly output) along the flight tracks on 9, 10, and 11 April 2008 (Fig. 7). The time series of measured $PM_{2.5}$ shows plumes containing enhanced aerosols were encountered during the flights. Aerosol mass in plumes ranged from 3 to 16 $\mu g\,m^{-3}$, while background levels were $\sim 1\,\mu g\,m^{-3}$. It should be noted that clean Arctic background and marine boundary layer air were less frequently sampled due to the planned flight patterns, which targeted anthropogenic and biomass burning influenced plumes. Gray shading denotes periods when in-situ measurements are not available, usually due to the presence of clouds.

Air mass origins indicated on Fig. 7 are determined using a combination of WRF-Chem and FLEXPART-WRF (simulations described below). The influence of anthropogenic and biomass burning emissions on the flight track is estimated using the NOANTHRO and NOFIRE sensitivity runs. Specifically, this influence is deemed significant if aerosol mass increased by more than 20 % upon including either anthropogenic or biomass burning emissions, according to the ratios [CTL $PM_{2.5}$]/[NOANTHRO

PM$_{2.5}$] and [CTL PM$_{2.5}$]/[NOFIRE PM$_{2.5}$]. The values of these ratios along the three flight tracks are presented in the Supplement, Fig. S2. On Fig. 7, pink shading indicates that the modeled PM$_{2.5}$ are influenced by European Anthropogenic emissions. Yellow shading indicates portions of the flight influenced by both biomass burning and anthropogenic emissions (mixed plumes). It should be noted that portions of the flight track that are influenced by biomass burning emissions are also influenced by anthropogenic emissions. Green shading indicates that the modeled air mass is significantly influenced by the domain northern boundary conditions (i.e. air transported from Asia). This influence is identified using FLEXPART-WRF, run in backwards mode with particles released every minute along the flight tracks (30 km × 30 km horizontally by 400 m vertically). When the FLEXPART-WRF retroplume mean trajectory passes closer than 5 grid cells (150 km) from the northern end of the domain, the air mass is considered as influenced by the northern boundary conditions. The typical transport pathway of such a plume is shown in the Supplement, Fig. S3. Finally, white shading indicates air masses that are not attributed to a specific source using the methods described above and are referred to as background air.

In the free troposphere, the model is able to reproduce the background PM$_{2.5}$ levels and the main peaks observed in European air masses for all three flights. The Normalized Mean Bias for PM$_{2.5}$ for all three flights, excluding background Arctic air and boundary condition air, is +8.8 %. Peaks attributed to European anthropogenic emissions are reproduced, although the model cannot capture some small-scale features due to its resolution. At the end of the 9 April flight, two concentrated plumes were sampled in situ around 12:00 and 12:15 UTC. The model identifies these plumes as mixed (anthropogenic/biomass burning), meaning that significant (> 40 %) enhancements in modeled PM$_{2.5}$ at these times are due to biomass burning or anthropogenic European emissions. The first PM$_{2.5}$ peak is underestimated by the model (around 12:00 UTC), and the second plume (around 12:15 UTC) is located 1.5 km too low in altitude. This may be due to uncertainties in the injection height for fires or in the intensity and timing of the emissions. However, the issue does not appear to be systematic in our simulation

because mixed plume peaks and enhancements are correctly represented during the 11 April flight. Modeled anthropogenic $PM_{2.5}$ are underestimated below 1 km at the beginning and end of the 11 April flight above Sweden (discussed in detail in Sect. 5.3). Plumes coming from the northern domain boundary, which are not studied in detail here, reflect the aerosols present in the MOZART 4 simulation used as the boundary conditions and point to a general underestimation, a feature seen in many global aerosol transport models. On 9 April, WRF-Chem also reproduces a large $PM_{2.5}$ peak located in the marine boundary layer. This peak is composed of more than 95 % sea salt in the model, and corresponds to sea spray uplifted by the strong 20 m s^{-1} winds present in the marine boundary layer in the region of the flight.

The modeled composition of $PM_{2.5}$ aerosols in anthropogenic and mixed polluted air masses is presented in Table 2. On 9 and 10 April, anthropogenic plumes are mostly composed of nitrate, sulfate and ammonium aerosol. Mixed plumes contain relatively less nitrate, but more sulfate, organic carbon, and black carbon. The proportion of sulfate is higher in mixed plumes than in anthropogenic plumes, despite the fact that sulfate and SO_2 emissions from biomass burning emissions are low. We show in the next section focused on plume origins that the proportion of sulfate is high for mixed plumes because they originate in a region of high anthropogenic SO_2 emissions. On 11 April, the composition of anthropogenic plumes and mixed plumes are similar, except for organic carbon, which is still lower in anthropogenic plumes. In Sect. 4, we showed that the model was overestimating nitrate and ammonium at the surface, while probably underestimating organic matter in the European source regions. Measurements of aerosol chemical composition are not available along the POLARCAT-France flights, but we can assume that similar biases apply to the modeled aerosol composition in the Arctic. The proportion of black carbon is 2.5 % in anthropogenic air masses (2.6 % for submicron particles), and 3 % in mixed plumes (3.1 % for submicron particles). These values are comparable with results from Brock et al. (2011), a study that found on average 2.4 % submicron mass of BC in anthropogenic plumes and 3.5 % in fire plumes in the Alaskan Arctic during spring 2008.

Aerosol optical and microphysical properties are very sensitive to their size distributions (Boucher, 1998; Dusek et al., 2006). To ensure that aerosol impacts are treated accurately in the CTL simulation, modeled aerosol number size distributions are validated against in situ measurements for selected plumes. Those plumes are indicated in each panel on Fig. 7 by ticks (referring to the modeled aerosol peak). 4 anthropogenic plumes (I, J, M, N) and 3 mixed plumes (K, L, O) are investigated. In the case of plume K, the modeled plume peak is located 1 km lower in the model than in observations, which results in it being displaced later in time along the flight track. For this plume, we compare the modeled and measured plumes using the peak aerosol mass encountered in the model (12:19 UTC) and measurements (12:14 UTC) respectively. This comparison is shown in Fig. 8. It indicates that the model adequately represents the aerosol size distributions with three exceptions. First, the model overestimates the number of large particles in the 9 April anthropogenic plumes (I, J). Second, the model cannot be compared to measurements in the smallest MOSAIC bin (aerosols 39 to 78 nm), due to the fact that the model does not resolve explicitly nucleation, but relies on a parameterization for nucleation and growth of particles with diameters less than 39 nm. Third, number concentrations are overestimated in the 2nd smallest MOSAIC bin (aerosols 78 to 156 nm) for mixed plumes (K and L–O) but not for anthropogenic plumes. We show in Sect. 5.2 that mixed plumes are ∼ 2 days older than anthropogenic plumes. This means that this overestimation is probably caused by underestimated growth processes, which have the largest impact on older plumes. However, aerosol optical properties are mostly sensitive to particles in the accumulation mode, which is correctly reproduced for all plumes.

5.2 Origins and transport pathways of anthropogenic and biomass burning plumes sampled during POLARCAT-France

Different types of aerosols transported to the Arctic during POLARCAT-France display different physical properties and vertical distributions. We investigate how different plume origins and transport pathways result in different aerosol properties in the Arctic.

28350

We focus on the role of wet scavenging during transport, which is the largest source of uncertainty in the representation of Arctic aerosols (Schwarz et al., 2010; Browse et al., 2012). Figure 9 shows typical plume transport pathways of an anthropogenic plume (plume J, Fig. 9a and c) and a mixed plume (plume K, Fig. 9b and d) measured during the campaign. Figure 9a and b shows the 0–20 km column of FLEXPART-WRF PES integrated for 7 days for both plumes. It indicates that anthropogenic plumes were mostly influenced by sources in central Europe 2–3 days prior to the measurements, while the mixed plume is 3 to 5 days old and under the influence of emissions in a large large region over eastern Europe and western Russia. This region corresponds to the location of agricultural fires in early April 2008, as well as significant anthropogenic emissions, especially of SO_2, as seen in Fig. 2. The larger age of mixed plumes explain why their size distribution is shifted toward larger sizes than younger anthropogenic plumes, as discussed in Quennehen et al. (2012).

Figure 9c and d show the mean altitude for each plume as a function of age. The anthropogenic plume experienced a rapid uplift from 1.5 to 6.5 km over Poland and the North Sea on 7 or 8 April, associated with the surface low over this region, while the mixed plume was transported to the Arctic below 2 km and slowly uplifted. Between 9 April and 11 April, FLEXPART-WRF trajectories (not shown here) inform us that mixed plume K mixed with air from fresher anthropogenic plumes I and J. This mixing explains why the chemical composition of the 11 April mixed plumes, showed in Table 2 and discussed above, is intermediate between 9 April mixed plume K and the 9 April anthropogenic plumes I and J.

The magnitude of wet scavenging along transport, also represented on Fig. 9c and d, is estimated using the difference between CTL PM_{10} minus NOWETSCAV PM_{10} along the retroplumes positions. As expected, strong PM_{10} depletions, reaching $-12\,\mu g\,m^{-3}$ ($-74\,\%$) are associated with precipitation during uplift of the anthropogenic plume in the frontal system over Poland, between 37 and 46 h before it was measured. Although the mixed plume does not experience such a rapid uplift, aerosols are also scavenged by rainout over Finland, between 35 and 45 h before sampling, decreasing PM_{10} levels by

$17 \, \mu g \, m^{-3}$ (−55 %). The accumulated precipitation in the simulation, compared to the E-OBS European daily gridded precipitation dataset (Haylock et al., 2008), shows that while WRF-Chem correctly reproduces the precipitation patterns observed during this period, it generally underestimates their intensity (see Supplement, Fig. S4). However, we have shown that average $PM_{2.5}$ levels are well reproduced in the source regions and in the Arctic, indicating that losses along transport are relatively well reproduced. This could be explained by compensations between underestimated precipitations and an overestimated wet scavenging rate in our simulation. An overestimation of the wet scavenging rate could be caused by the overestimated hygroscopy of the modeled aerosol, which contains too much ammonium and nitrate, and not enough organic matter.

5.3 Vertical aerosol distributions: 9 April 2008

The vertical structure of aerosol layers transported to the Arctic is often complex (Brock et al., 2011), and the vertical distribution of absorbing aerosol layers can have a large influence on their radiative effects (e.g. Meloni et al., 2005; Raut and Chazette, 2008). Here, the modeled vertical structure of aerosol layers in the Arctic troposphere is evaluated using the pseudo backscatter ratio at 532 nm (PBR) measured by the airborne LIDAR shooting at nadir. The measured PBR is represented in Fig. 10b for the 9 April flight, clouds and data below clouds are masked in white. The altitude of the aircraft, which was going north to south and returning to Kiruna, is shown as a black line on panels B to E. We choose to show the 9 April flight because modeled low-level pollution is not influenced by the model northern boundary conditions on this day. The model to observations comparison is therefore not affected by the performance of the global model MOZART4. Figure 10a shows the $PM_{2.5}$ measured in situ by the aircraft during the same period. The $PM_{2.5}$ and LIDAR-derived PBR just below the aircraft present a very similar evolution: the $PM_{2.5}$ and PBR signals are enhanced during the whole leg between 4 and 5 km, at the aircraft altitude and just below. This good correlation be-

tween aerosol mass and optical properties allows us to validate aerosol concentrations vertical distributions through their optical properties.

The PBR at 532 nm is compared to cross-sections of the simulated backscatter ratio (Fig. 10c) simulated PM$_{2.5}$ (Fig. 10d) and simulated aerosol number concentration (Fig. 10e) extracted along flight tracks from the WRF-Chem simulation. The magnitude of the PBR is correctly reproduced, with background regions between 1 and 1.1, and visible aerosol layers reaching values of 1.3 to 1.5. Peak intensities in plumes transported to the Arctic region tend to be underestimated by the model, as the modeled plumes are too diluted vertically. Plume locations are reasonably well reproduced with an enhanced layer at 5 km during the whole flight leg, and two main layers at lower latitudes and altitudes, between 1.5–2 and 3–4 km. One enhanced layer measured between 11:30 and 11:50 UTC at 1 km is missing from the modeled ASPR cross-section because it is displaced ∼ 50 km to the southwest in the simulation (see Supplement, Fig. S5). This displacement is probably due to the cumulative effect of small errors on wind speed and wind direction over the 3 to 5 days of long-range transport. The model underestimates the PBR in the intense layer measured in situ and by the LIDAR at 5 km at 12:00 UTC, which is in agreement with the underestimation observed on PM$_{2.5}$ levels previously described in Fig. 7. This layer, identified as a 5-day-old mixed plume in the model, features low PM$_{2.5}$ but high aerosol number concentration (Fig. 10e), suggesting it is mostly composed of small particles. This means that the discrepancy in this layer probably corresponds to underestimated condensation processes in the aerosol model. This is in agreement with the comparison of the modeled and observed size distributions of aerosols in mixed plumes, discussed in Sect. 5.1, which indicated underestimated particle growth in the older mixed plumes.

We investigate the vertical distribution of modeled anthropogenic and biomass burning aerosols during this profile, and the impact of wet scavenging on the vertical distribution. Figure 11 shows the sensitivity of the PM$_{2.5}$ vertical cross section to anthropogenic emissions (Fig. 11a), biomass burning emissions (Fig. 11b) and wet scavenging (Fig. 11c). During the 9 April flight, anthropogenic emissions have the largest

influence in the mid to upper troposphere, above 4 km and in the PBL and lower troposphere, below 2 km, while the impacts of biomass burning emissions are more pronounced between 2 and 4 km. Figure 11b confirms that the plume missing at 5 km in Fig. 10c is indeed due to biomass burning emissions, but the associated enhancement above background is very low, around $1 \, \mu g \, m^{-3}$. According to Fig. 11c, this low enhancement is not due to high wet scavenging in this layer. As discussed before, this confirms that the underestimation of $PM_{2.5}$ in this layer may be due to insufficient condensation. The impact of wet scavenging is the strongest for the lower level mixed pollution, as discussed in the case of plume K in Fig. 9d. It is negligible in biomass burning layers located between 2 and 4 km, and strong relatively to total $PM_{2.5}$ in the southernmost and low-altitude anthropogenic layer.

6 Impacts of European aerosol transport on the Arctic

Results presented so far give us confidence in the way this transport event is represented in our simulation in terms of meteorology, $PM_{2.5}$ levels, size distributions, spatial extent and vertical structure of the plumes We now investigate the regional impacts of this transport event in the European Arctic region. Figure 12 shows the average vertical profiles of the modeled anthropogenic and biomass burning contributions to $PM_{2.5}$ (total and chemically speciated) north of the Arctic circle (within the model domain) during the period from 00:00 UTC 8 April, to 00:00 UTC 12 April. The very low aerosol concentrations are due to area-weighted averaging of European enhancements confined in the lower Scandinavian Arctic with the rest of the clean Arctic region contained in the domain. Because of this, we will not discuss the absolute enhancements and instead focus on relative values. This average profile shows the same general features than what was observed in-situ and by LIDAR during POLARCAT-France, with anthropogenic emissions separated between a low altitude (1.5 km) and a high altitude (4.5 km) contribution, and biomass burning emissions impacting intermediate altitudes (2.5–3 km). Different species display different vertical structures: for the anthropogenic

Transport of European aerosols to the Arctic in spring

L. Marelle et al.

Title Page

Abstract | Introduction

Conclusions | References

Tables | Figures

|◀ | ▶|

◀ | ▶

Back | Close

Full Screen / Esc

Printer-friendly Version

Interactive Discussion

CC BY

contribution, BC, OC, and $SO_4^=$ are enhanced at low altitudes. This corresponds to the mixed layers from eastern Europe and Russia. High altitude anthropogenic plumes from central Europe contain enhanced NH_4^+, NO_3^- and BC. Biomass burning plumes contain larger mass fractions of BC and OC than anthropogenic plumes, and BC and OC influence lower altitudes than other $PM_{2.5}$ species from biomass burning. These results are in agreement with earlier studies by Stohl et al. (2007) and Lund Myhre et al. (2007), who analyzed cases of transport of biomass burning plumes from eastern Europe to the Arctic in spring 2006. Using FLEXPART simulations and LIDAR measurements, they showed that biomass burning aerosols were mostly confined below 3 km altitudes in the Arctic. Fischer et al. (2011) investigated aerosol transport from the mid-latitudes to the Arctic during April 2008 with the global chemical transport model GEOS-Chem, and found that in the high Arctic (75–85° N), NH_4^+ and $SO_4^=$ were sensitive to European anthropogenic emissions at all altitudes, with a peak sensitivity between 2 and 5 km.

Pueschel and Kinne (1995) have shown that layers of aerosols containing black carbon, even with very high single scattering albedos (0.98), could warm the atmosphere over snow or ice covered surfaces. Because the transport of pollution from Europe to the Arctic is especially efficient in late winter and early spring when the Scandinavian snow cover is still extensive, aerosols transported to the Scandinavian Arctic should contribute to enhanced local atmospheric heating rates in this region. Figure 13a shows the direct and semi-direct shortwave (0.125 to 10 µm wavelengths) radiative effect (DSRE) of aerosols at the Top Of Atmosphere (TOA), in regions significantly influenced by in-domain anthropogenic and biomass burning emissions. The DSRE is estimated by taking the difference between the upward short wave TOA flux calculated online by the Goddard shortwave module within WRF-Chem, in the CTL simulation minus the NODIRECT simulation. Because WRF-Chem upward radiative fluxes are by convention always negative, positive DSRE values at TOA indicate heating of the surface–atmosphere column. The DSRE is averaged over the period from 00:00 UTC 8 April to 00:00 UTC 12 April. In-domain anthropogenic and biomass burning emissions

Transport of European aerosols to the Arctic in spring

L. Marelle et al.

Title Page

Abstract	Introduction
Conclusions	References
Tables	Figures

|◀ | ▶|

◀ | ▶

Back | Close

Full Screen / Esc

Printer-friendly Version

Interactive Discussion

are considered significant if the $PM_{2.5}$ column sensitivity to anthropogenic and biomass burning emissions (shown in Fig. 13b) exceeds 50 % of the total column of CTL $PM_{2.5}$. We added this condition to exclude from our calculation of the DSRE the areas where the dominant contribution is due to aerosols originating from the boundary conditions (i.e. the Asian plume), from natural emissions (i.e. sea salt) or from background levels.

As expected, the DSRE is negative over land and ocean where snow and ice cover are low, but positive over regions with high snow and ice covers (see the snow and ice cover map on Fig. 13c). The 4 day average value of the DSRE at TOA north of 60° N in regions significantly influenced by European pollution is shown in Table 3. In addition to the total average effect north of 60° N, we compute values for the DSRE over surfaces with extensive snow and ice cover (> 90 %), and over the ocean surface. On average, the European aerosols have a cooling effect north of 60° N ($-0.98\,\mathrm{W\,m}^{-2}$). Over snow and ice, the average DSRE is $+0.58\,\mathrm{W\,m}^{-2}$, peaking near $+2\,\mathrm{W\,m}^{-2}$ over a large region in northern Scandinavia where aerosol optical depths (AOD) are the highest (~ 0.5 at 400 nm). The DSRE is much lower over the Russian snowpack east of 42° E because the European mixed air mass in this region is either optically shallow (AOD from 0.05 to 0.2) or is located below clouds. Over the Arctic seas, the DSRE is negative due to the lower albedo of the ocean surface. The calculated DSRE in oceanic regions north of 60° N influenced by the European plumes is $-1.5\,\mathrm{W\,m}^{-2}$. Minimum values reach close to $-5\,\mathrm{W\,m}^{-2}$ over the Norwegian Sea close to the coast of Norway, where the cloud cover is the lowest, as shown in Fig. 13d.

Brock et al. (2011) calculated a direct radiative effect of $+3.3\,\mathrm{W\,m}^{-2}$ over snow at TOA for the average of 10 typical polluted profiles measured during the ARCPAC campaign, not taking the semi-direct effect into account. Maximum modeled BC in WRF-Chem along the POLARCAT-France flight tracks is $150\,\mathrm{ng\,m}^{-3}$ (anthropogenic) and $260\,\mathrm{ng\,m}^{-3}$ (mixed fire/anthropogenic), which are comparable with the average BC values reported for anthropogenic ($148\,\mathrm{ng\,m}^{-3}$) and fire plumes ($312\,\mathrm{ng\,m}^{-3}$) in Brock et al. (2011). This means that on average, the BC values for pollution-influenced plumes in our simulation are lower than values reported by Brock et al. (2011). Quinn

et al. (2007) found a similar direct radiative effect value of $+2.5\,W\,m^{-2}$ over snow at TOA for the average polluted conditions encountered during the Arctic haze maximum at Barrow. Those results were obtained at solar noon, in clear sky conditions, over snow and in polluted regions only, conditions that lead to a maximum direct effect. Using a similar approach, we compute the DSRE in regions influenced by European pollution, close to noon (11:00 UTC), and above high snow covers ($> 90\,\%$). This results in an average DSRE of $+1.9\,W\,m^{-2}$ north of $60°\,N$. If we exclude the snowpack in Russia, east of $42°\,E$, the average DSRE in reaches $+3.3\,W\,m^{-2}$. These values are in agreement with results from Brock et al. (2011) and Quinn et al. (2007). It should be noted that our retrievals are done in all-sky conditions and not exactly at local solar noon, introducing a slight low bias. Including the semi-direct effect in our calculations might have introduced a warming bias, which would be limited by the nudging of WRF-Chem temperature, relative humidity and wind speed towards FNL reanalyzes in the free troposphere. We verified that differences in cloud cover between the NODIRECT and CTL simulations were limited in magnitude and extent, with only a few local points over the sea affected (below $10\,\%$ cloud cover change for the 8 to 12 April average), that mostly cancel each other out when regionally averaged.

Lund Myhre et al. (2007) calculated the direct forcing of biomass burning aerosols transported from Europe to the Arctic in late April and early May 2006 from space borne aerosol optical depth measurements. For those exceptionally intense plumes, they found that the cooling direct effect at TOA reached $-35\,W\,m^{-2}$ over the regions with the highest AOD in the Barents Sea, while the maximum warming direct effect over snow was limited to $+5\,W\,m^{-2}$ over Svalbard. Keeping in mind that our results are not directly comparable because of the different times of year and different averaging periods, we found a 4 day average direct and semi-direct effect reaching maximum values of $+2\,W\,m^{-2}$ over snow-covered Scandinavia, and maximum cooling values of $-5\,W\,m^{-2}$ over the Norwegian Sea. Several reasons could explain this different balance between warming and cooling effects. In our case, modeled European plumes contained higher levels of black carbon (2.5 to $3\,\%$ of submicron aerosol mass) than

the measured value used in the study of Lund Myhre et al. (1.98 %). The transport event studied here also featured a high altitude anthropogenic plume that would have a local warming effect above the high albedo low-level clouds. The inclusion of the semi-direct effect in our study might have also played a limited role.

At the surface, the direct aerosol effect causes local cooling for all types of land surfaces, but we also showed that BC was especially enhanced at the surface in anthropogenic and biomass burning plumes, which could lead to surface warming through snow albedo effects of BC deposited on snow. This effect is not taken into account in our simulation, but an earlier study by Wang et al. (2011) showed that during spring 2008 (April–May), significant levels of anthropogenic BC (1 to $5\,\mathrm{mg\,C\,m^{-2}\,month^{-1}}$) were deposited on snow in Northern Europe, leading to 1 to 2 % changes of the regional albedo of snow and ice.

7   Summary and conclusions

In this study, we investigate an aerosol transport event from Europe to the European Arctic using measurements as well as regional chemical-transport model simulations for the first time. Specifically, an event involving long-range transport of biomass burning and anthropogenic aerosols from Europe to the Arctic in April 2008 is studied using the regional model WRF-Chem (8 bin MOSAIC aerosol scheme), to quantify impacts on aerosol concentrations and resulting direct shortwave radiative effects in the Scandinavian Arctic. Modeled aerosols are evaluated against ground-based observations from the EMEP network in European source regions, and using POLARCAT-France aircraft measurements aloft in the European Arctic. The model reproduces background $PM_{2.5}$ levels at EMEP ground based stations in Europe (NMB = −0.9 %) and in Arctic polluted air masses measured by the ATR42 aircraft (NMB = +8.8 %). Comparison with EMEP measurements shows that the model overestimates concentrations of particulate NO_3^- (NMB = +107 %) and NH_4^+ (NMB = +53 %) in source regions, probably be-

cause of overestimated NH_3 emissions, and may underestimate OC. Good agreement is found between simulated $SO_4^=$ and EMEP measurements (NMB = −0.6 %).

The model indicates that European biomass burning and anthropogenic emissions both had a significant influence on total aerosol mass concentrations (> 20 % of total PM$_{2.5}$) during portions of the POLARCAT-France spring campaign measurements analyzed in this study. Plumes influenced by biomass burning sources in the model are also found to be significantly influenced by anthropogenic emissions. These modeled mixed plumes contain elevated organic carbon and black carbon concentrations. They originated in Eastern Europe and Western Russia, and followed low altitude (below 2 km) transport pathways into the Arctic. Significant wet scavenging is predicted in the model during transport over Finland, reducing PM$_{10}$ levels by 55 %. Modeled high-altitude anthropogenic plumes, originating in central Europe, were rapidly uplifted (from 1 to 6 km in less than 24 h) by warm conveyor belt circulations over Poland and the North Sea. The model also predicts significant wet scavenging during transport of these anthropogenic plumes (PM$_{10}$ reduced by 74 %). Evaluation of the model against in-situ measurements and LIDAR profiles below the aircraft shows that the model correctly represents the average vertical distribution of aerosols during this European transport event, as well as the magnitude of the aerosol optical properties. However, this comparison suggests that the model is under representing the rate of aerosol growth processes, especially condensation, which has the largest impact on the older mixed plumes (3 to 5 days old).

The model is used to investigate the average vertical structure of aerosol enhancements from European anthropogenic and biomass burning emissions in the Scandinavian Arctic. Anthropogenic emissions are shown to influence aerosols at both low (∼ 1.5 km) and higher altitudes (∼ 4.5 km), while biomass burning emissions influence aerosols between these altitudes (2.5 to 3 km). BC and $SO_4^=$ aerosol concentrations are proportionally more enhanced at lower altitudes, including at the surface.

This transport event brought elevated aerosol concentrations north of the Arctic Circle for a rather short period of 4 days, from 8 to 12 April 2008. Due to the location of the

polar front, these European aerosols did not mix significantly with local Arctic air further north. However, this event is particularly interesting because of the extensive seasonal snow cover present in Northern Scandinavia during this period. We show that the event had a significant local atmospheric warming effect over snow and ice surfaces. The average 96 h TOA direct and semi-direct shortwave radiative effect from this event over snow and sea ice is found to be +0.58 W m^{-2} north of 60° N. At solar noon, in regions significantly influenced by European aerosols, larger warming is predicted, +3.3 W m^{-2} (TOA direct and semi-direct radiative effects) over the Scandinavian and Finnish snow cover north of 60° N. This result is of the same order of magnitude as values previously reported for aerosols in the western Artic (Brock et al., 2011; Quinn et al., 2007).

These radiative effect values do not include the impacts of cloud/aerosol interactions, which could be quite large and compensate the warming effect of European aerosols over snow and ice-covered surfaces. This indirect aerosol effect is still uncertain, especially in the Arctic, and further work is needed to estimate its magnitude. During POLARCAT-France, the ATR-42 aircraft also sampled an intense Asian plume that was not investigated in this study, which focuses on European aerosols. The contribution of Asian sources to Arctic pollution is an active area of research, and the POLARCAT-France dataset, as well as the other POLARCAT datasets, could be the basis of a focused study on the transport of such plumes to the Arctic.

The Supplement related to this article is available online at doi:10.5194/acpd-14-28333-2014-supplement.

References

Ackerman, A. S., Toon, O. B., Stevens, D. E., Heymsfield, A. J., Ramanathan, V., and Welton, E. J.: Reduction of tropical cloudiness by soot, Science, 288, 1042–1047, doi:10.1126/science.288.5468.1042, 2000.

Ancellet, G., Pelon, J., Blanchard, Y., Quennehen, B., Bazureau, A., Law, K. S., and Schwarzenboeck, A.: Transport of aerosol to the Arctic: analysis of CALIOP and French aircraft data during the spring 2008 POLARCAT campaign, Atmos. Chem. Phys., 14, 8235–8254, doi:10.5194/acp-14-8235-2014, 2014.

Barrie, L. A.: Arctic air pollution: an overview of current knowledge, Atmos. Environ., 20, 643–663, 1986.

Bond, T. C., Habib, G., and Bergstrom, R. W.: Limitations in the enhancement of visible light absorption due to mixing state, J. Geophys. Res., 111, D20211, doi:10.1029/2006JD007315, 2006.

Boucher, O.: On aerosol direct shortwave forcing and the Henyey–Greenstein phase function, J. Atmos. Sci., 55, 128–134, 1998.

Brioude, J., Arnold, D., Stohl, A., Cassiani, M., Morton, D., Seibert, P., Angevine, W., Evan, S., Dingwell, A., Fast, J. D., Easter, R. C., Pisso, I., Burkhart, J., and Wotawa, G.: The Lagrangian particle dispersion model FLEXPART-WRF version 3.1, Geosci. Model Dev., 6, 1889–1904, doi:10.5194/gmd-6-1889-2013, 2013.

Brock, C. A., Cozic, J., Bahreini, R., Froyd, K. D., Middlebrook, A. M., McComiskey, A., Brioude, J., Cooper, O. R., Stohl, A., Aikin, K. C., de Gouw, J. A., Fahey, D. W., Ferrare, R. A., Gao, R.-S., Gore, W., Holloway, J. S., Hübler, G., Jefferson, A., Lack, D. A., Lance, S., Moore, R. H., Murphy, D. M., Nenes, A., Novelli, P. C., Nowak, J. B., Ogren, J. A., Peischl, J., Pierce, R. B., Pilewskie, P., Quinn, P. K., Ryerson, T. B., Schmidt, K. S., Schwarz, J. P., Sodemann, H., Spackman, J. R., Stark, H., Thomson, D. S., Thornberry, T., Veres, P., Watts, L. A.,

|◄ | ►|

◄ | ►

Back | Close

Full Screen / Esc

Printer-friendly Version

Interactive Discussion

Discussion Paper | Discussion Paper | Discussion Paper | Discussion Paper | Discussion Paper

Warneke, C., and Wollny, A. G.: Characteristics, sources, and transport of aerosols measured in spring 2008 during the aerosol, radiation, and cloud processes affecting Arctic Climate (ARCPAC) Project, Atmos. Chem. Phys., 11, 2423–2453, doi:10.5194/acp-11-2423-2011, 2011.

Browse, J., Carslaw, K. S., Arnold, S. R., Pringle, K., and Boucher, O.: The scavenging processes controlling the seasonal cycle in Arctic sulphate and black carbon aerosol, Atmos. Chem. Phys., 12, 6775–6798, doi:10.5194/acp-12-6775-2012, 2012.

Charlson, R. J., Schwartz, S. E., Hales, J. M., Cess, R. D., Coakley, J. A., Hansen, J. E., and Hofmann, D. J.: Climate forcing by anthropogenic aerosols, Science, 255, 423–430, 1992.

Chen, F. and Dudhia, J.: Coupling an advanced land surface hydrology model with the Penn State-NCAR MM5 modeling system. Part I: Model implementation and sensitivity, Mon. Weather Rev., 129, 569–585, doi:10.1175/1520-0493(2001)129<0569:CAALSH>2.0.Co;2, 2001.

Chou, M.-D. and Suarez, M. J.: A Solar Radiation Parameterization (CLIRAD-SW) for Atmospheric Studies, NASA/TM-1999-104606, 15, 48 pp., 1999.

Dernier van der Gon, H. D., Hendriks, C., Kuenen, J., Segers, A., and Visschedijk, A.: Description of Current Temporal Emission Patterns and Sensitivity of Predicted AQ for Temporal Emission Patterns, EU FP7 MACC deliverable report D_D-EMIS_1.3, 2011.

de Villiers, R. A., Ancellet, G., Pelon, J., Quennehen, B., Schwarzenboeck, A., Gayet, J. F., and Law, K. S.: Airborne measurements of aerosol optical properties related to early spring transport of mid-latitude sources into the Arctic, Atmos. Chem. Phys., 10, 5011–5030, doi:10.5194/acp-10-5011-2010, 2010.

Dusek, U., Frank, G. P., Hildebrandt, L., Curtius, J., Schneider, J., Walter, S., Chand, D., Drewnick, F., Hings, S., Jung, D., Borrmann, S., and Andreae, M. O.: Size matters more than chemistry for cloud-nucleating ability of aerosol particles, Science, 312, 1375–1378, 2006.

Emmons, L. K., Walters, S., Hess, P. G., Lamarque, J.-F., Pfister, G. G., Fillmore, D., Granier, C., Guenther, A., Kinnison, D., Laepple, T., Orlando, J., Tie, X., Tyndall, G., Wiedinmyer, C., Baughcum, S. L., and Kloster, S.: Description and evaluation of the Model for Ozone and Related chemical Tracers, version 4 (MOZART-4), Geosci. Model Dev., 3, 43–67, doi:10.5194/gmd-3-43-2010, 2010.

Fahey, K. M. and Pandis, S. N.: Optimizing model performance: variable size resolution in cloud chemistry modelling, Atmos. Environ., 35, 4471–4478, 2001.

Fast, J. D., Gustafson Jr., W. W. I., Easter, R., Zaveri, R. A., Barnard, J. C., Chapman, E. G., Grell, G., and Peckham, S.: Evolution of ozone, particulates, and aerosol direct radiative forcing in the vicinity of Houston using a fully coupled meteorology-chemistry-aerosol model, J. Geophys. Res., 111, D21305, doi:10.1029/2005JD006721, 2006.

Fast, J. D., Gustafson Jr., W. I., Berg, L. K., Shaw, W. J., Pekour, M., Shrivastava, M., Barnard, J. C., Ferrare, R. A., Hostetler, C. A., Hair, J. A., Erickson, M., Jobson, B. T., Flowers, B., Dubey, M. K., Springston, S., Pierce, R. B., Dolislager, L., Pederson, J., and Zaveri, R. A.: Transport and mixing patterns over Central California during the carbonaceous aerosol and radiative effects study (CARES), Atmos. Chem. Phys., 12, 1759–1783, doi:10.5194/acp-12-1759-2012, 2012.

Fisher, J. A., Jacob, D. J., Wang, Q., Bahreini, R., Carouge, C. C., Cubison, M. J., Dibb, J. E., Diehl, T., Jimenez, J. L., Leibensperger, E. M., Lu, Z., Meinders, M. B. J., Pye, H. O. T., Quinn, P. K., Sharma, S., Streets, D. G., van Donkelaar, A., and Yantosca, R. M.: Sources, distribution, and acidity of sulfate-ammonium aerosol in the Arctic in winter–spring, Atmos. Environ., 45, 7301–7318, doi:10.1016/j.atmosenv.2011.08.030, 2011.

Flamant, C. and Pelon, J.: Atmospheric boundary-layer structure over the Mediterranean during a Tramontane event, Q. J. Roy. Metor. Soc., 122, 1741–1778, 1996.

Flanner, M. G., Zender, C. S., Randerson, J. T., and Rasch, P. J.: Present-day climate forcing and response from black carbon in snow, J. Geophys. Res., 112, D11202, doi:10.1029/2006JD008003, 2007.

Freitas, S. R., Longo, K. M., Chatfield, R., Latham, D., Silva Dias, M. A. F., Andreae, M. O., Prins, E., Santos, J. C., Gielow, R., and Carvalho Jr., J. A.: Including the sub-grid scale plume rise of vegetation fires in low resolution atmospheric transport models, Atmos. Chem. Phys., 7, 3385–3398, doi:10.5194/acp-7-3385-2007, 2007.

Garrett, T. J. and Zhao, C.: Increased Arctic cloud longwave emissivity associated with pollution from mid-latitudes, Nature, 440, 787–789, doi:10.1038/nature04636, 2006.

Garrett, T. J., Brattstrom, S., Sharma, S., Worthy, D. E. J., and Novelli, P.: The role of scavenging in the seasonal transport of black carbon and sulfate to the Arctic, Geophys. Res. Lett., 38, L16805, doi:10.1029/2011gl048221, 2011.

Greenaway, K. R.: Experiences with Arctic flying weather, Royal Meteorol. Soc. Can. Branch, Toronto, Ont., Canada, 1950.

Grell, G. A. and Devenyi, D.: A generalized approach to parameterizing convection combining ensemble and data assimilation techniques, Geoph. Res. Let., 29, 38-1–38-4, doi:10.1029/2002GL015311, 2002.

Grell, G. A., Peckham, S. E., Schmitz, R., McKeen, S. A., Frost, G., Skamarock, W. C., and Eder, B.: Fully coupled "online" chemistry within the WRF model, Atmos. Environ., 39, 6957–6975, 2005.

Guenther, A., Karl, T., Harley, P., Wiedinmyer, C., Palmer, P. I., and Geron, C.: Estimates of global terrestrial isoprene emissions using MEGAN (Model of Emissions of Gases and Aerosols from Nature), Atmos. Chem. Phys., 6, 3181–3210, doi:10.5194/acp-6-3181-2006, 2006.

Gustafson, W. I., Qian, Y., and Fast, J. D.: Downscaling aerosols and the impact of neglected subgrid processes on direct aerosol radiative forcing for a representative global climate model grid spacing, J. Geophys. Res., 116, D13303, doi:10.1029/2010JD015480, 2011.

Haylock, M., Hofstra, N., Klein Tank, A., Klok, E., Jones, P., and New, M. A.: European daily high-resolution gridded data set of surface temperature and precipitation for 1950–2006, J. Geophys. Res., 113, D20119, doi:10.1029/2008JD010201, 2008.

Haywood, J. M. and Shine, K. P.: The effect of anthropogenic sulfate and soot aerosol on the clear sky planetary radiation budget, Geophys. Res. Lett., 22, 603–606, 1995.

Hodzic, A., Jimenez, J. L., Madronich, S., Canagaratna, M. R., DeCarlo, P. F., Kleinman, L., and Fast, J.: Modeling organic aerosols in a megacity: potential contribution of semi-volatile and intermediate volatility primary organic compounds to secondary organic aerosol formation, Atmos. Chem. Phys., 10, 5491–5514, doi:10.5194/acp-10-5491-2010, 2010.

Iversen, T. and Joranger, E.: Arctic air pollution and large scale atmospheric flows, Atmos. Environ., 19, 2099–2108, 1985.

Jacobson, M. Z.: Short term effects of controlling fossil fuel soot, biofuel soot and gases, and methane on climate, Arctic ice, and air pollution health, J. Geophys. Res., 115, D14209, doi:10.1029/2009JD013795, 2010.

Janjic, Z. I.: The step-mountain eta coordinate model: further developments of the convection, viscous sublayer, and turbulence closure schemes, Mon. Weather Rev., 122, 927–945, 1994.

Law, K. S., Stohl, A., Quinn, P. K., Brock, C., Burkhart, J., Paris, J.-D., Ancellet, G., Singh, H. B., Roiger, A., Schlager, H., Dibb, J., Jacob, D. J., Arnold, S. R., Pelon, J., and Thomas, J. L.: Arctic air pollution: new insights from POLARCAT-IPY, B. Am. Meteorol. Soc., doi:10.1175/BAMS-D-13-00017.1, early online releases, 2014.

Title Page

Abstract | Introduction

Conclusions | References

Tables | Figures

|◄ | ►|

◄ | ►

Back | Close

Full Screen / Esc

Printer-friendly Version

Interactive Discussion

Lund Myhre, C., Toledano, C., Myhre, G., Stebel, K., Yttri, K. E., Aaltonen, V., Johnsrud, M., Frioud, M., Cachorro, V., de Frutos, A., Lihavainen, H., Campbell, J. R., Chaikovsky, A. P., Shiobara, M., Welton, E. J., and Tørseth, K.: Regional aerosol optical properties and radiative impact of the extreme smoke event in the European Arctic in spring 2006, Atmos. Chem. Phys., 7, 5899–5915, doi:10.5194/acp-7-5899-2007, 2007.

Meloni, D., di Sarra, A., Di Iorio, T., and Fiocco, G.: Influence of the vertical profile of Saharan dust on the visible direct radiative forcing, J. Quant. Spectrosc. Ra., 93, 397–413, 2005.

Meng, Z., Dabdub, D., and Seinfeld, J. H.: Chemical coupling between atmospheric ozone and particulate matter, Science, 277, 116–119, 1997.

Mitchell, J. M.: Visual range in the polar regions with particular reference to the Alaskan Arctic, J. Atmos. Terr. Phys. Spec., Suppl., 1, 195–211, 1957.

Mlawer, E. J., Taubman, S. J., Brown, P. D., Iacono, M. J., and Clough, S. A.: Radiative transfer for inhomogeneous atmospheres: RRTM, a validated correlated-k model for the longwave, J. Geophys. Res., 102, 16663–16682, 1997.

Morrison, H., Thompson, G., and Tatarskii, V.: Impact of cloud microphysics on the development of trailing stratiform precipitation in a simulated squall line: comparison of one and two-moment schemes, Mon. Weather Rev., 137, 991–1007, doi:10.1175/2008mwr2556.1, 2009.

Murrells, T. P., Passant, N. R., Thistlethwaite, G., Wagner, A., Li, Y., Bush, T., Norris, J., Coleman, P. J., Walker, C., Stewart, R. A., Tsagatakis, I., Conolly, C., Brophy, N. C. J., and Okamura, S.: UK Emissions of Air Pollutants 1970 to 2007, AEAa, 2010.

Nicolet, M.: On the molecular scattering in the terrestrial atmosphere: an empirical formula for its calculation in the homosphere, Planet. Space Sci., 32, 1467–1468, 1984.

Pilinis, C., Pandis, S. N., and Seinfeld, J. H.: Sensitivity of direct climate forcing by atmospheric aerosols to aerosol size and composition, J. Geophys. Res., 100, 18739–18754, 1995.

Pueschel, R. F. and Kinne, S. A.: Physical and radiative properties of Arctic atmospheric aerosols, Sci. Total Environ., 161, 811–824, 1995.

Quennehen, B., Schwarzenboeck, A., Schmale, J., Schneider, J., Sodemann, H., Stohl, A., Ancellet, G., Crumeyrolle, S., and Law, K. S.: Physical and chemical properties of pollution aerosol particles transported from North America to Greenland as measured during the POLARCAT summer campaign, Atmos. Chem. Phys., 11, 10947–10963, doi:10.5194/acp-11-10947-2011, 2011.

Title Page

Abstract | Introduction

Conclusions | References

Tables | Figures

|◄ | ►|

◄ | ►

Back | Close

Full Screen / Esc

Printer-friendly Version

Interactive Discussion

Quennehen, B., Schwarzenboeck, A., Matsuki, A., Burkhart, J. F., Stohl, A., Ancellet, G., and Law, K. S.: Anthropogenic and forest fire pollution aerosol transported to the Arctic: observations from the POLARCAT-France spring campaign, Atmos. Chem. Phys., 12, 6437–6454, doi:10.5194/acp-12-6437-2012, 2012.

Quinn, P. K., Miller, T. L., Bates, T. S., Ogren, J. A., Andrews, E., and Shaw, G. E.: A three-year record of simultaneously measured aerosol chemical and optical properties at Barrow, Alaska, J. Geophys. Res., 107 (D11), 4130, doi:10.1029/2001JD001248, 2002.

Quinn, P. K., Shaw, G., Andrews, E., Dutton, E. G., Ruoho-Airola, T., and Gong, S. L.: Arctic haze: current trends and knowledge gaps, Tellus B, 59, 99–114, 2007.

Rahn, K. A.: Relative importances of North America and Eurasia sources of arctic aerosol, Atmos. Environ., 15, 1447–1455, doi:10.1016/0004-6981(81)90351-6, 1981.

Rahn, K. A., Borys, R. D., and Shaw, G. E.: Asian source of Arctic haze bands, Nature, 268, 713–715, 1977.

Raut, J.-C. and Chazette, P.: Radiative budget in the presence of multi-layered aerosol structures in the framework of AMMA SOP-0, Atmos. Chem. Phys., 8, 6839–6864, doi:10.5194/acp-8-6839-2008, 2008.

Sessions, W. R., Fuelberg, H. E., Kahn, R. A., and Winker, D. M.: An investigation of methods for injecting emissions from boreal wildfires using WRF-Chem during ARCTAS, Atmos. Chem. Phys., 11, 5719–5744, doi:10.5194/acp-11-5719-2011, 2011.

Schwarz, J. P., Spackman, J. R., Gao, R. S., Watts, L. A., Stier, P., Schulz, M., Davis, S. M., Wofsy, S. C., and Fahey, D. W.: Global-scale black carbon profiles observed in the remote atmosphere and compared to models, Geophys. Res. Lett., 37, L18812, doi:10.1029/2010GL044372, 2010.

Schwarzenboeck, A., Heintzenberg, J., and Mertes, M.: Incorporation of aerosol particles between 25 and 850 nm into cloud element: measurements with a new complementary sampling system, Atmos. Res., 52, 241–260, 2000.

Shaw, G. E: The Arctic haze phenomenon, B. Am. Meteorol. Soc., 76, 2403–2413, 1995.

Shindell, D. and Faluvegi, G.: Climate response to regional radiative forcing during the twentieth century, Nat. Geosci., 2, 294–300, doi:10.1038/NGEO473, 2009.

Stohl, A.: Characteristics of atmospheric transport into the Arctic troposphere, J. Geophys. Res., 111, D11306, doi:10.1029/2005JD006888, 2006.

Title Page

Abstract | Introduction

Conclusions | References

Tables | Figures

|◄ | ►|

◄ | ►

Back | Close

Full Screen / Esc

Printer-friendly Version

Interactive Discussion

Stohl, A., Forster, C., Frank, A., Seibert, P., and Wotawa, G.: Technical note: The Lagrangian particle dispersion model FLEXPART version 6.2, Atmos. Chem. Phys., 5, 2461–2474, doi:10.5194/acp-5-2461-2005, 2005.

Stohl, A., Berg, T., Burkhart, J. F., Fjǽraa, A. M., Forster, C., Herber, A., Hov, Ø., Lunder, C., McMillan, W. W., Oltmans, S., Shiobara, M., Simpson, D., Solberg, S., Stebel, K., Ström, J., Tørseth, K., Treffeisen, R., Virkkunen, K., and Yttri, K. E.: Arctic smoke – record high air pollution levels in the European Arctic due to agricultural fires in Eastern Europe in spring 2006, Atmos. Chem. Phys., 7, 511–534, doi:10.5194/acp-7-511-2007, 2007.

Toon, O. B. and Ackerman, T. P.: Algorithms for the calculation of scattering by stratified spheres, Appl. Optics, 20, 3657–3660, 1981.

Tuccella, P., Curci, G., Visconti, G., Bessagnet, B., Menut, L., and Park, R. J.: Modeling of gas and aerosol with WRF/Chem over Europe: evaluation and sensitivity study, J. Geophys. Res., 117, D03303, doi:10.1029/2011JD016302, 2012.

Thomas, J. L., Raut, J.-C., Law, K. S., Marelle, L., Ancellet, G., Ravetta, F., Fast, J. D., Pfister, G., Emmons, L. K., Diskin, G. S., Weinheimer, A., Roiger, A., and Schlager, H.: Pollution transport from North America to Greenland during summer 2008, Atmos. Chem. Phys., 13, 3825–3848, doi:10.5194/acp-13-3825-2013, 2013.

Twomey, S.: The influence of pollution on the shortwave albedo of clouds, J. Atmos. Sci., 34, 1149–1152, doi:10.1175/1520-0469(1977)034<1149:TIOPOT>2.0.CO;2, 1977.

Wang, H., Easter, R. C., Rasch, P. J., Wang, M., Liu, X., Ghan, S. J., Qian, Y., Yoon, J.-H., Ma, P.-L., and Vinoj, V.: Sensitivity of remote aerosol distributions to representation of cloud–aerosol interactions in a global climate model, Geosci. Model Dev., 6, 765–782, doi:10.5194/gmd-6-765-2013, 2013.

Wang, Q., Jacob, D. J., Fisher, J. A., Mao, J., Leibensperger, E. M., Carouge, C. C., Le Sager, P., Kondo, Y., Jimenez, J. L., Cubison, M. J., and Doherty, S. J.: Sources of carbonaceous aerosols and deposited black carbon in the Arctic in winter-spring: implications for radiative forcing, Atmos. Chem. Phys., 11, 12453–12473, doi:10.5194/acp-11-12453-2011, 2011.

Warneke, C., Bahreini, R., Brioude, J., Brock, C. A., de Gouw, J. A., Fahey, D. W., Froyd, K. D., Holloway, J. S., Middlebrook, A., Miller, L., Montzka, S., Murphy, D. M., Peischl, J., Ryerson, T. B., Schwarz, J. P., Spackman, J. R., and Veres, P.: Biomass burning in Siberia and Kazakhstan as an important source for haze over the Alaskan Arctic in April 2008, Geophys. Res. Lett., 36, L02813, doi:10.1029/2008GL036194, 2009.

Title Page

Abstract | Introduction

Conclusions | References

Tables | Figures

|◄ | ►|

◄ | ►

Back | Close

Full Screen / Esc

Printer-friendly Version

Interactive Discussion

Warneke, C., Froyd, K. D., Brioude, J., Bahreini, R., Brock, C. A., Cozic, J., de Gouw, J. A., Fahey, D. W., Ferrare, R., Holloway, J. S., Middlebrook, A. M., Miller, L., Montzka, S., Schwarz, J. P., Sodemann, H., Spackman, J. R., and Stohl, A.: An important contribution to springtime Arctic aerosol from biomass burning in Russia, Geophys. Res. Lett., 37, L01801, doi:10.1029/2009gl041816, 2010.

Wexler, A. S., Lurmann, F. W., and Seinfeld, J. H.: Modelling urban and regional aerosols – I. Model development, Atmos. Environ., 28, 531–546, 1994.

Wiedinmyer, C., Quayle, B., Geron, C., Belote, A., McKenzie, D., Zhang, X., O'Neill, S., Klos, K., and Wynne, K. K.: Estimating emissions from fires in North America for air quality modelling, Atmos. Environ., 40, 3419–3432, 2006.

Wiedinmyer, C., Akagi, S. K., Yokelson, R. J., Emmons, L. K., Al-Saadi, J. A., Orlando, J. J., and Soja, A. J.: The Fire INventory from NCAR (FINN): a high resolution global model to estimate the emissions from open burning, Geosci. Model Dev., 4, 625–641, doi:10.5194/gmd-4-625-2011, 2011.

Wild, O., Zhu, X., and Prather, M. J.: Fast-J: accurate simulation of in- and below-cloud photolysis in tropospheric chemical models, J. Atmos. Chem., 37, 245–282, 2000.

Zaveri, R. and Peters, L. K.: A new lumped structure photochemical mechanism for large-scale applications, J. Geophys. Res., 104, 30387–30415, 1999.

Zaveri, R. A., Easter, R. C., Fast, J. D., and Peters, L. K.: Model for Simulating Aerosol Interactions and Chemistry (MOSAIC), J. Geophys. Res., 113, D13204, doi:10.1029/2007JD008792, 2008.

Transport of European aerosols to the Arctic in spring

L. Marelle et al.

Title Page

Abstract	Introduction
Conclusions	References
Tables	Figures

|◄ | ►|

◄ | ►

Back | Close

Full Screen / Esc

Printer-friendly Version

Interactive Discussion

Table 1. Parameterizations and options used for the WRF-Chem simulations.

Atmospheric process	WRF-Chem option
Planetary Boundary Layer	MYJ (Janjic et al., 1994)
Surface layer	Monin–Obukhov Janjic Eta scheme (Janjic et al., 1994)
Land surface	Unified Noah land-surface model (Chen and Dudhia, 2001)
Microphysics	Morrison (Morrison, Thompson and Tatarskii, 2009)
SW radiation	Goddard (Chou and Suarez, 1999)
LW radiation	RRTM (Mlawer et al., 1997)
Photolysis	Fast-J (Wild et al., 2000)
Cumulus parameterization	Grell-3 (Grell and Devenyi, 2002)
Gas phase chemistry	CBM-Z (Zaveri and Peters, 1999)
Aerosol model	MOSAIC 8 bins (Zaveri et al., 2008)

Transport of European aerosols to the Arctic in spring

L. Marelle et al.

Table 2. Modeled PM$_{2.5}$ aerosol composition by source type along POLARCAT-France spring flights. BC, OC and SS are black carbon, organic carbon, and sea salt, respectively.

Flight	Source type	BC (%)	OC (%)	$SO_4^=$ (%)	NH_4^+ (%)	NO_3^- (%)	SS (%)
9 Apr 2008	Anthro.	2.5	7.0	24.1	20.6	40.2	5.6
	Mixed fires + anthro.	3.2	12.6	35.0	20.1	26.0	3.2
10 Apr 2008	Anthro.	2.3	5.5	21.7	20.9	42.4	7.3
11 Apr 2008	Anthro.	2.7	8.7	34.4	19.5	27.3	7.4
	Mixed fires + anthro.	2.8	11.9	33.9	19.4	28.5	3.4

Table 3. 4 day average shortwave direct and semi-direct effect (DSRE) at top of atmosphere (TOA) north of 60° N, over regions significantly influenced by European pollution (> 50 % of total $PM_{2.5}$ column due to in-domain anthropogenic and biomass burning emissions).

Type of land surface	DSRE at TOA $(W\,m^{-2})$
Snow and Ice cover > 90 %	+0.58
Ocean	−1.52
All	−0.98
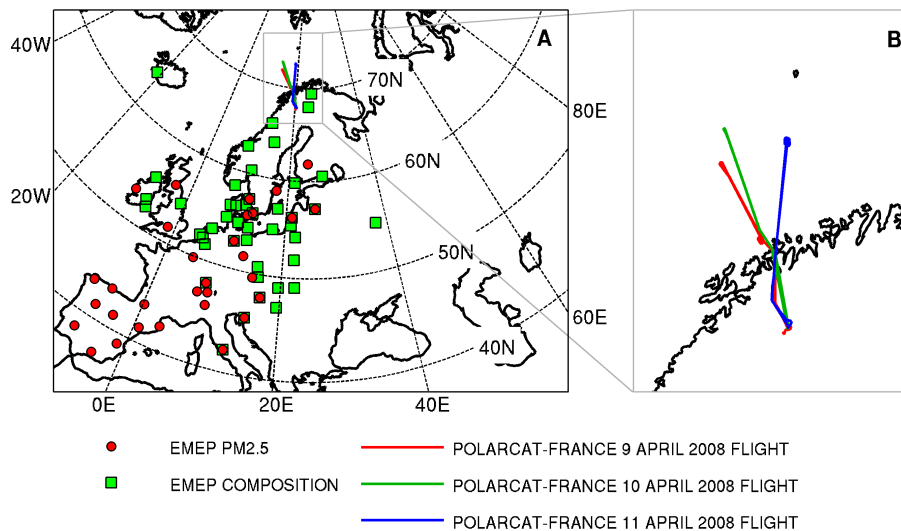
Figure 1. (a) WRF-Chem domain including the location of ground based EMEP measurement stations used for this study. Stations measuring $PM_{2.5}$ are marked by a red circle, and stations measuring aerosol composition are marked by a green square. Stations with both measurements are indicated with both symbols. The POLARCAT-France spring flight tracks are shown in red, green and blue, with a zoom in over the flight region shown in **(b)**.

Title Page

Abstract | Introduction

Conclusions | References

Tables | Figures

|◄ | ►|

◄ | ►

Back | Close

Full Screen / Esc

Printer-friendly Version

Interactive Discussion
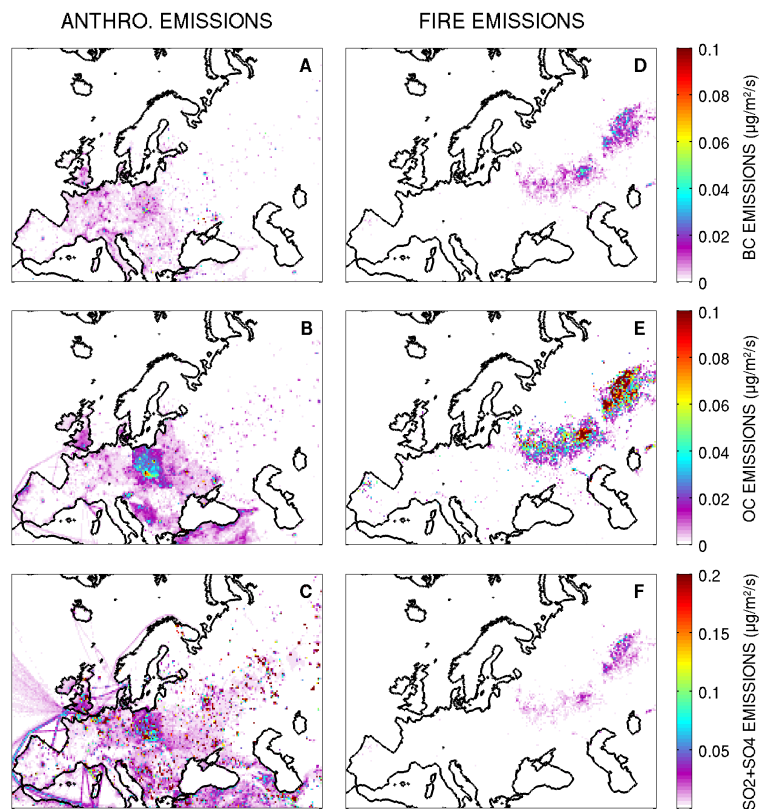
Figure 2. Averaged emissions within the model domain during the simulation period (1 April 2008–12 April 2008) due to anthropogenic activities (HTAP v2) and biomass burning (FINN v1). Anthropogenic BC, OC, and $SO_2 + SO_4$ emissions are shown in **(a–c)** and biomass burning BC, OC and $SO_2 + SO_4$ emissions are shown in **(d–f)**.
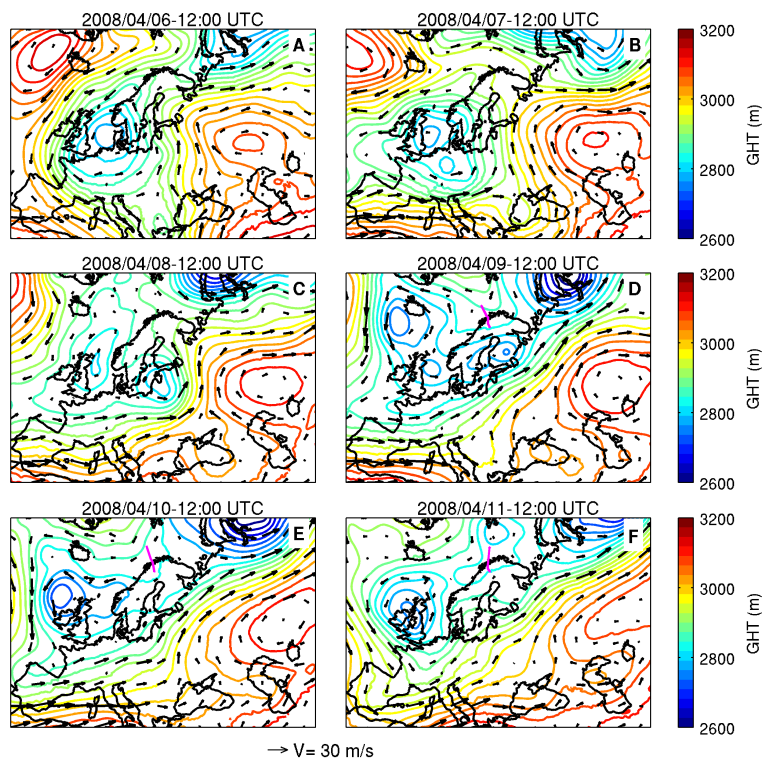
Figure 3. Meteorological situation simulated by WRF-Chem during the POLARCAT-France spring campaign period, represented by the 700 hPa geopotential height (contour lines) and 700 hPa wind vectors ($30 \, \text{m s}^{-1}$ vector given for scale) on 6–11 April 2008 (12:00 UTC). The POLARCAT-France flight tracks on 9, 10, and 11 April 2008 are indicated in magenta.
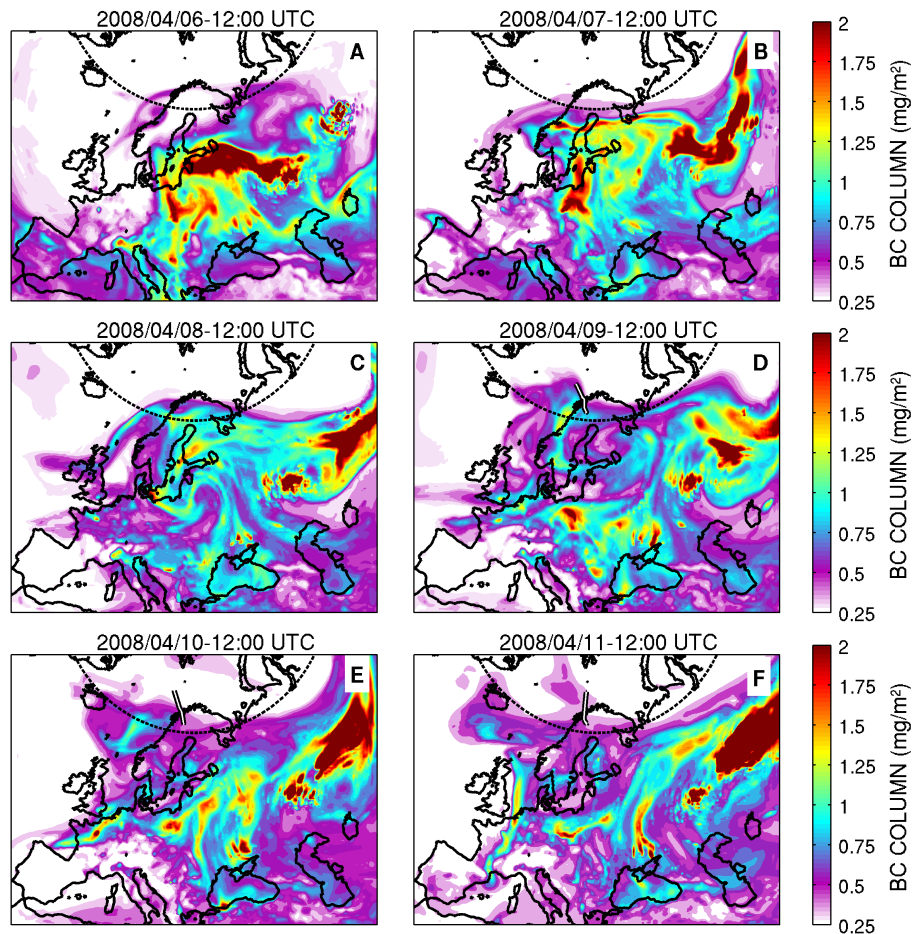
Figure 4. Simulated BC column on 6–11 April 2008 (12:00 UTC). POLARCAT-France flight tracks are indicated in white, with a black border.

Title Page

Abstract | Introduction

Conclusions | References

Tables | Figures

Back | Close

Full Screen / Esc

Printer-friendly Version

Interactive Discussion
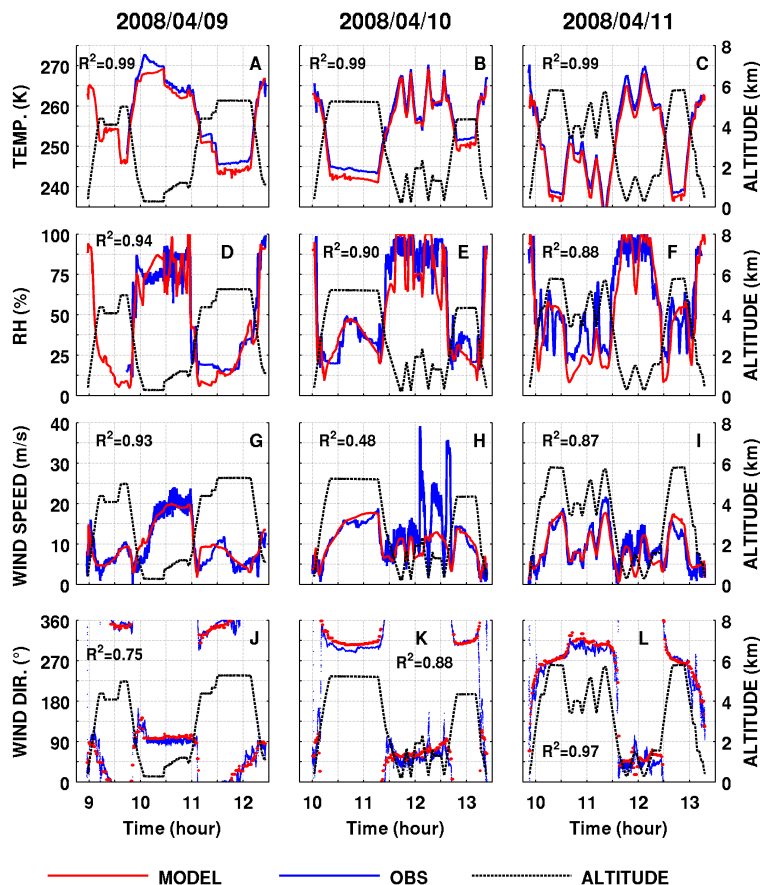
Figure 5. Time series of modeled (red) and measured (blue) **(a–c)** temperature, **(d–f)** relative humidity, **(g–i)** wind speed, and **(j–l)** wind direction extracted along the POLARCAT-France flight tracks. The corresponding aircraft altitude is shown in black.
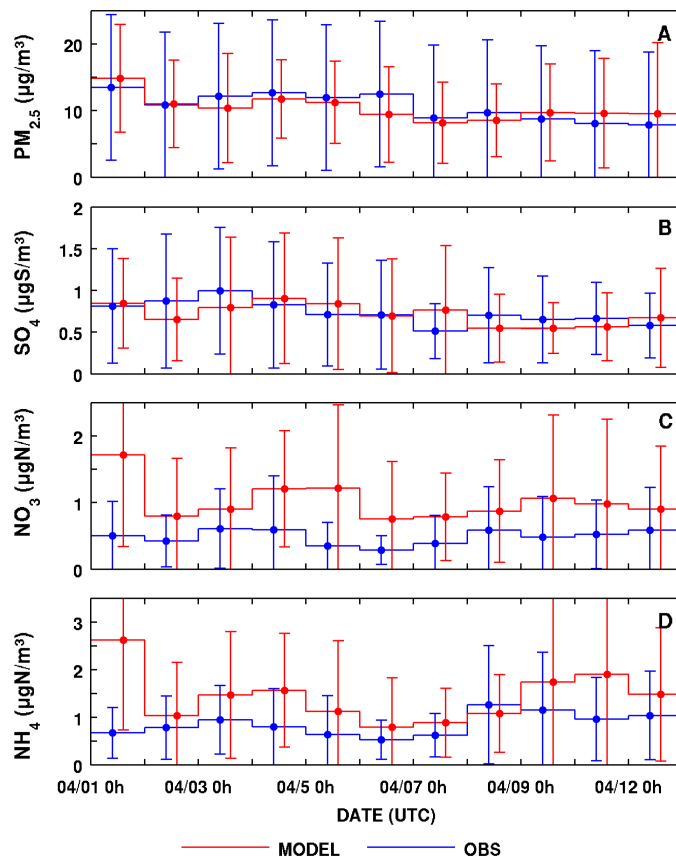
Figure 6. Daily mean aerosol mass measured at EMEP stations within the domain (in blue) and WRF-Chem aerosol mass extracted at the position of the stations (in red) for **(a)** $PM_{2.5}$, **(b)** sulfate aerosol, **(c)** nitrate aerosol, **(d)** ammonium aerosol. The standard deviation between stations is indicated by the error bars.

Title Page

Abstract | Introduction

Conclusions | References

Tables | Figures

|◀ | ▶|

◀ | ▶

Back | Close

Full Screen / Esc

Printer-friendly Version

Interactive Discussion
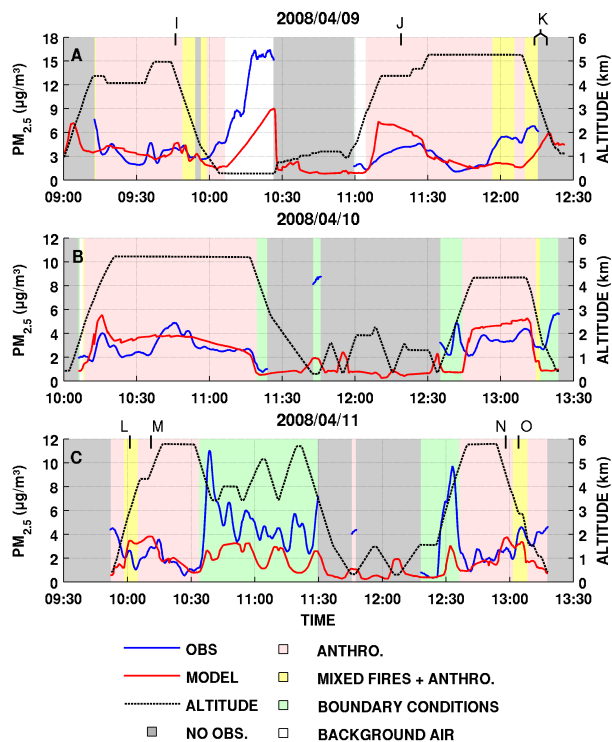
Figure 7. Time series of $PM_{2.5}$ measured during POLARCAT-France (blue) and modeled (red) with the aircraft altitude indicated in black for the three POLARCAT-France flights on **(a)** 9 April 2008, **(b)** 10 April 2008 and **(c)** 11 April 2008. Grey shading indicates times when no measurements are available. Colors indicate when $PM_{2.5}$ was significantly influenced ($> 20\%$ of $PM_{2.5}$) by source: green = air entering the domain from the northern boundary conditions, pink = anthropogenic emissions within the domain, yellow = fire emissions within the domain. Letter labels indicate anthropogenic (I, J, M, N) and mixed anthropogenic/fire (K, L, O) plumes investigated further.
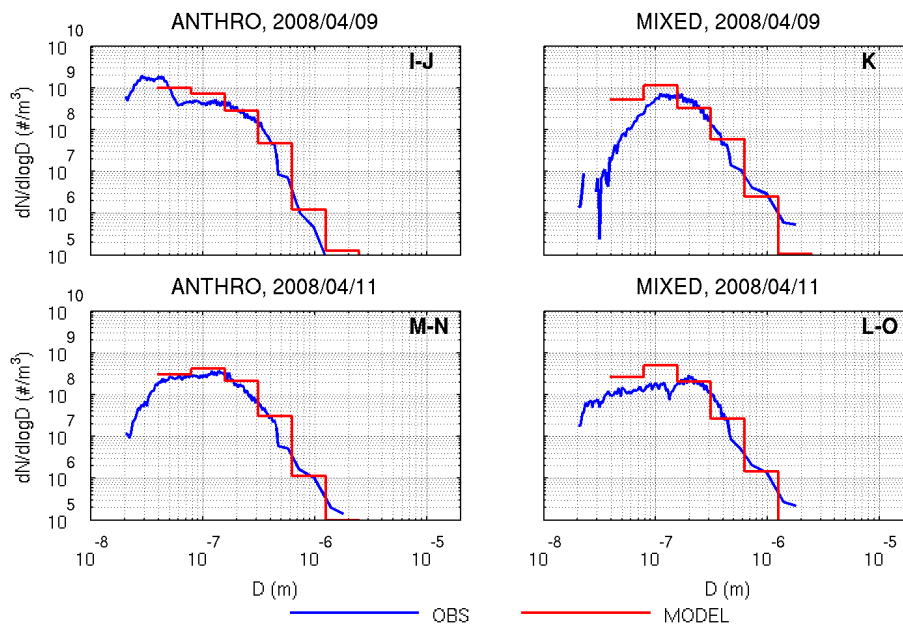
Figure 8. Modeled (red) and measured (blue) number size distributions of plumes labeled (I–O) in Fig. 7, influenced by (I, J, M, N) European anthropogenic and (K, L, O) mixed European anthropogenic and fire emissions. Modeled and observed size distributions corresponding to two consecutive samplings of the same plume during the same flight (I–J, M–N, L–O) were averaged together.
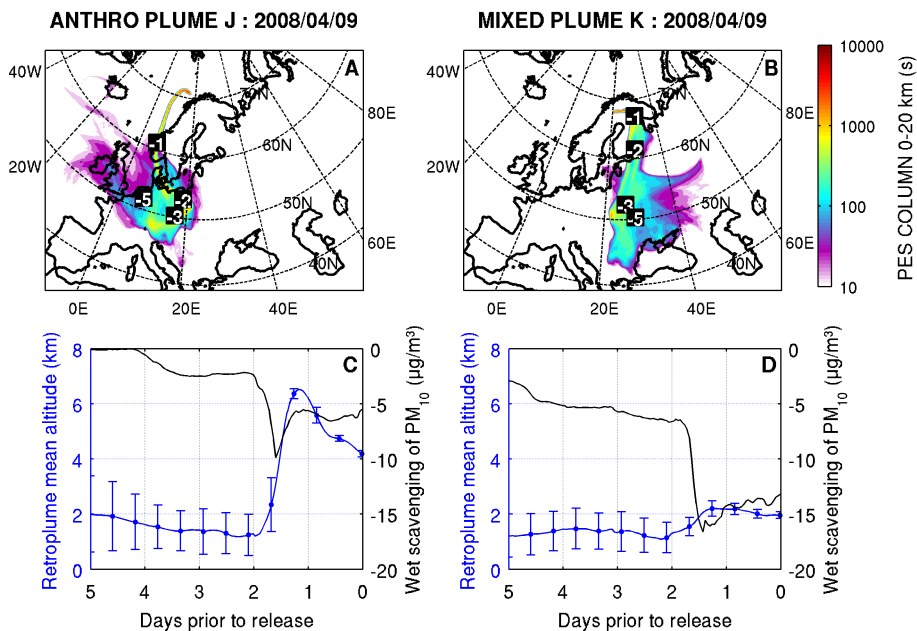
Figure 9. Backward mode FLEXPART-WRF column integrated PES (**a** and **b**) showing typical transport pathways for an anthropogenic plume (left, plume J, originating on 9 April 2008 at 11:19 UTC on the POLARCAT flight track) and a mixed anthropogenic/biomass-burning plume (right, plume K, originating on 9 April 2008 at 12:19 UTC on the flight track). (**c** and **d**) show each plume's mean altitude with RMS error bars showing vertical dispersion (blue) and the difference between the CTL PM_{10} and the NOWETSCAV PM_{10} along transport, indicating wet scavenging events (black).

Title Page

Abstract | Introduction

Conclusions | References

Tables | Figures

|◄ | ►|

◄ | ►

Back | Close

Full Screen / Esc

Printer-friendly Version

Interactive Discussion
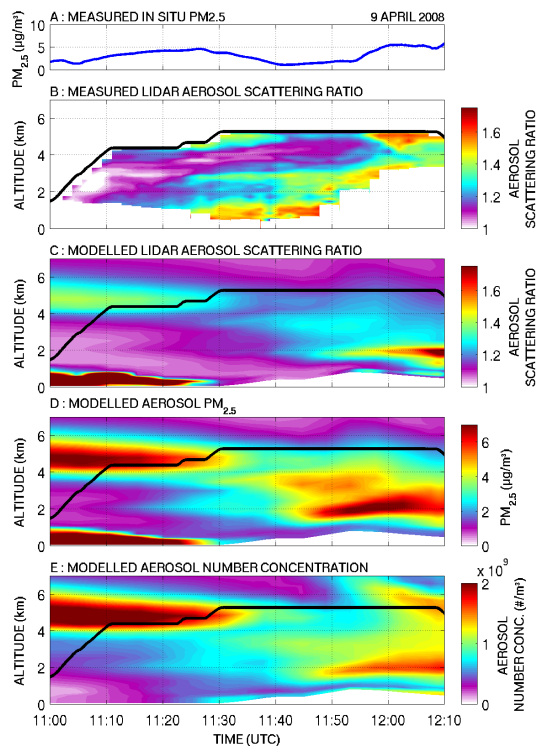
Figure 10. (a) PM$_{2.5}$ measured in situ during the last part of the 9 April 2008 flight, **(b)** LIDAR 532 nm pseudo backscatter ratio measured at nadir during the same portion of the flight (altitude in black, white areas represent topography or cloudy areas where no aerosol data is available), **(c)** simulated WRF-Chem LIDAR 532 nm pseudo backscatter ratio, **(d)** modeled PM$_{2.5}$ cross-section at the same position, **(e)** modeled aerosol number concentration cross-section at the same position.
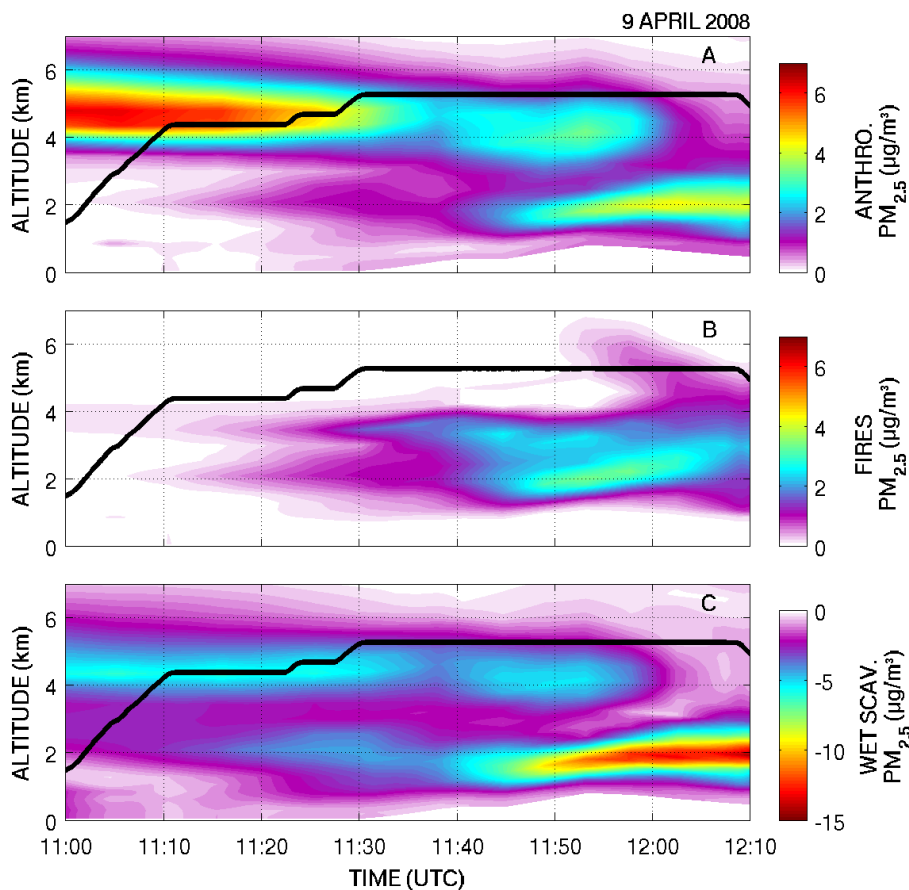
Figure 11. Modeled aerosol cross-sections along the flight track (plane altitude in black), showing the sensitivity of the modeled PM$_{2.5}$ to **(a)** anthropogenic emissions, **(b)** fire emissions, and **(c)** wet scavenging.

Title Page

Abstract | Introduction

Conclusions | References

Tables | Figures

|◄ | ►|

◄ | ►

Back | Close

Full Screen / Esc

Printer-friendly Version

Interactive Discussion
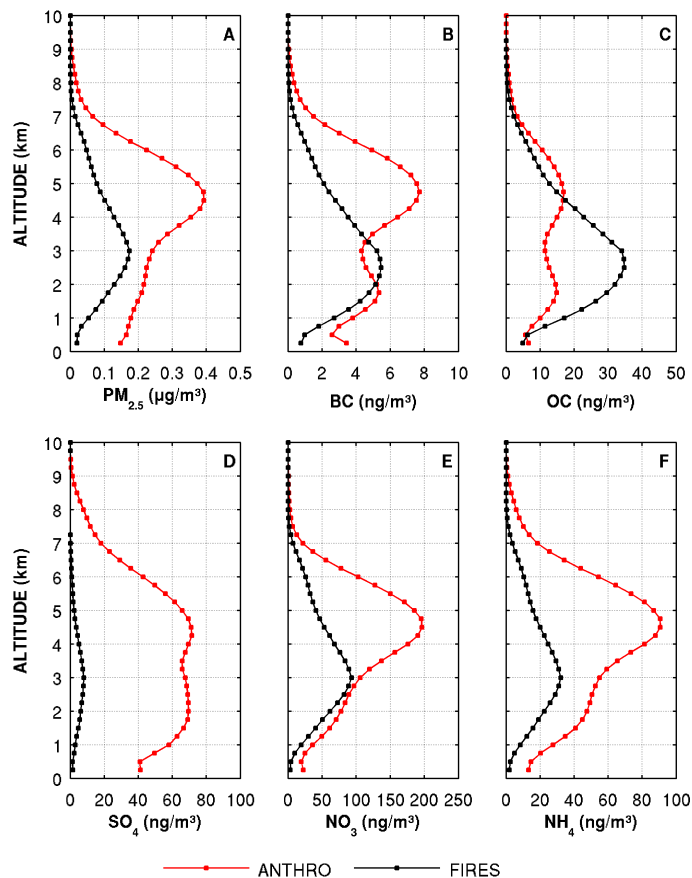
Figure 12. Modeled vertical profiles of enhancements in **(a)** $PM_{2.5}$, **(b)** BC, **(c)** OC, **(d)** $SO_4^=$, **(e)** NO_3^- and **(f)** NH_4^+ $PM_{2.5}$, due to anthropogenic (red) and fire (black) emissions within the WRF-Chem model domain, averaged in the Arctic (latitude > 66.6° N) and over the period from 00:00 UTC 8 April 2008 to 00:00 UTC 12 April 2008.

Title Page

Abstract | Introduction

Conclusions | References

Tables | Figures

|◀ | ▶|

◀ | ▶

Back | Close

Full Screen / Esc

Printer-friendly Version

Interactive Discussion
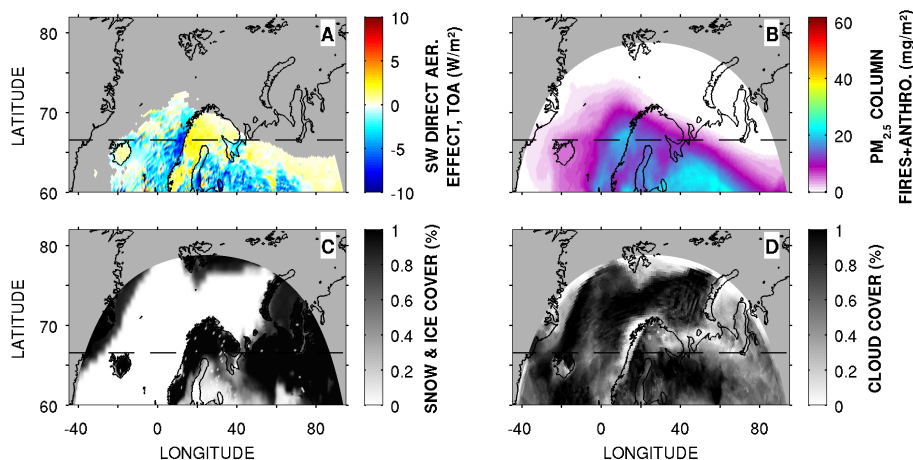
Figure 13. Model averages over the period from 00:00 UTC 8 April 2008 to 00:00 UTC 12 April 2008 of the: **(a)** aerosol direct and semi-direct radiative effect (DSRE), at Top Of Atmosphere (TOA), in regions significantly affected by in-domain anthropogenic and fire emissions, **(b)** PM$_{2.5}$ column sensitivity to anthropogenic and biomass burning emissions, **(c)** fractional snow and sea ice cover, **(d)** fractional cloud cover. In panel **(a)**, regions not significantly affected by in-domain emissions are masked in gray. In panels **(b–d)**, regions outside of the WRF-Chem domain are masked in gray. The Arctic Circle is indicated by a dashed line.

Full Screen / Esc

Printer-friendly Version

Interactive Discussion